New Zealand Journal of Geology and Geophysics

ROYAL SOCIETY TE APĀRANGI

RESEARCH ARTICLE OPEN ACCESS

Seismic Stratigraphy of Eocene–Recent Mixed Depositional Systems on the SE New Zealand Continental Margin, Great South Basin

Onyekachi N. Ibezim[1] | Dorrik Stow[1] | Uisdean Nicholson[1] | Sara Rodrigues[2]

[1]School of Energy, Geoscience, Infrastructure and Society, Heriot-Watt University, Edinburgh, UK | [2]Andalusian Earth Science Institute (IACT), Spanish National Research Council (CSIC), Granada, Spain

Correspondence: Dorrik Stow (d.stow@hw.ac.uk)

Received: 26 June 2025 | **Revised:** 29 September 2025 | **Accepted:** 30 October 2025

Keywords: Antarctic Circumpolar Current | mixed systems | morphological elements | Southland Current | turbidites–contourites

ABSTRACT

The continental margin of SE New Zealand is strongly influenced by the Southland Current and associated water masses. This new seismic stratigraphic study of the margin has revealed a range of depositional mounds and erosional channels that document the close interaction of turbidity and bottom currents in shaping the margin from the Mid-Eocene onward. Bottom-current influence was initiated with the onset of the Antarctic Circumpolar Current, following the opening of the Tasmanian Gateway. Following this event, four stages of evolution are identified: (1) the Mid-Eocene saw the onset of the first mixed depositional system with a series of levee-drifts adjacent to downslope channels, alongslope-oriented contourite-dominated drifts, and an alongslope contourite moat; (2) the Early to Late Oligocene saw the continued vertical growth and incision of these mixed depositional and erosional elements; (3) the Late Oligocene to Mid-Miocene saw a significant change to a more turbidite-dominated mixed system, with a weakened bottom-current influence; and (4) the Mid-Miocene to Recent saw a resumption in bottom-current activity, and development of a more contourite-dominated system. The changes observed in margin evolution reflect variations in tectonic activity and source area uplift, variation in continental slope topography, and evolving bottom-current systems.

1 | Introduction

Numerous continental margins, including those offshore Argentina, Nova Scotia, Brazil, Antarctic Peninsula, Mozambique and Tanzania, have a well-documented history of mixed depositional systems formed by the interaction between downslope gravity induced flows and alongslope bottom-current-driven circulation (Campbell and Mosher 2016; Chen et al. 2020; Fierens et al. 2019; Rodrigues, Deptuck, et al. 2022; Rodrigues et al. 2021; Uenzelmann-Neben 2006). These systems develop a broad spectrum of morphological features whose evolution is controlled by various combinations of erosion, deposition, and aggradation (Hernández-Molina et al. 2022b; Rodrigues, Hernández-Molina, et al. 2022). These processes shape the overall morphological character and modify the complex architecture of mixed depositional systems. The complex nature of their interactions makes it difficult to identify and characterize the sedimentary features in mixed depositional systems. However, most mixed depositional systems seem to comprise two categories of primary and secondary morphological features. The primary morphological features comprise four depositional elements: downslope elongated mounded drifts (e.g., Argentina, Nova Scotia, and Antarctic Peninsula), channel-drifts (e.g., South China Sea and Mozambique), elongated channel levees (e.g., SE Greenland, Weddell Sea, and SW Brazil) and reworked submarine fans or depositional lobes (e.g., Gulf of Mexico and SW Brazil (Fonnesu et al. 2020; Miramontes et al. 2021; Rodrigues, Hernández-Molina, et al. 2022; Rodrigues et al. 2021). The major erosional features consist of submarine channels and submarine canyons. The secondary morphological features include gravitational deposits, channel overbanks, sediment waves, scours, furrows, gullies, scarps, and terraces.

Much work has been done on the geometries of the main depositional and erosional features (Rodrigues, Hernández-Molina, et al. 2022). For example, their internal architectures may be differentiated into two main geometries: asymmetric or symmetric. These geometries are frequently constrained by the lateral migration of the system. In fact, several authors have observed that mixed systems may migrate down- or up-current (in relation to the bottom-current direction), due to spatial and temporal variations in bottom-current strength, gravitational flow frequency, and many other factors (Fonnesu et al. 2020; Gong et al. 2018). For instance, the studies done on the mixed systems of Mozambique, Tanzania, and Antarctic Peninsula reported an up-current migration (Fonnesu et al. 2020; Fuhrmann et al. 2020; Miramontes et al. 2021; Rebesco et al. 1998; Rebesco et al. 2002; Sansom 2018; Thiéblemont et al. 2020), whereas the works focused on the mixed systems of Uruguay, Argentina, South China Sea, and SE Greenland documented a down-current migration (Creaser et al. 2017; Gong, Wang, Zheng, et al. 2016; Gong et al. 2013; Rasmussen et al. 2003). Although seismic data provide valuable insight into the spatial and temporal evolution of mixed systems, the complexity and variability of these systems mean that many features and morphologies remain poorly documented, so clear and universally applicable diagnostic criteria at the seismic scale are still lacking (Fuhrmann et al. 2022; Pandolpho et al. 2021; Rodrigues, Hernández-Molina, et al. 2022), particularly in underexplored regions like the New Zealand margin.

The New Zealand continental margin provides an important opportunity to add to the repository of mixed systems, as it will allow us to better understand the processes involved in the formation and evolution of mixed deposits, further identify and characterize the spatiotemporal variability observed in mixed turbidite–contourite systems, and improve our knowledge on the role of bottom currents in continental margin construction. Southeast New Zealand uniquely combines a well-imaged mixed turbidite–contourite record with direct bottom-current influence (Carter, McCave, et al. 2004), turbidite systems (Carter and Carter 1996; Deng et al. 2024) and exceptional age control (Constable et al. 2013), which will allow us to resolve how changing alongslope currents shape downslope routing pathways and the seismic scale architecture of the Late Paleogene to Quaternary.

In this study, our primary aim is to characterize the large-scale mixed depositional system preserved in the Late Paleogene to Quaternary record of the southeast New Zealand margin in order to resolve the interactions between alongslope and downslope processes and thereby reconstruct paleo-oceanic circulation. This study also aims to shed light on the onset timing of the Antarctic Circumpolar Current (ACC). Earlier estimates proposed that the ACC began between 41 and 37 Ma (Barker et al. 2007; Nicholson and Stow 2019; Pfuhl and McCave 2005; Scher and Martin 2006). Importantly, the onset of the ACC marks the shift to ACC-dominated circulation, which established alongslope boundary conditions on the margin, making its timing essential for interpreting bottom-current strength relative to turbidity delivery and for decoding the stratigraphic architecture of the mixed system. In doing so, this article delivers the first holistic seismic and stratigraphic synthesis of the southeast New Zealand margin's Late Paleogene to Quaternary mixed turbidite–contourite system, defining its architecture and process interactions and advancing process-based models for its evolution.

To achieve these aims, we have defined the following objectives: (i) establish the seismic stratigraphy and chronostratigraphy of Mid-Eocene to Quaternary deposits; (ii) characterize the mixed depositional system with respect to its physiographic features, sedimentary stacking pattern, and distinct depositional and erosional features; (iii) constrain the precise timing of ACC onset on the margin; and (iv) interpret the depositional evolution and related palaeoceanographic changes along the southeast New Zealand Margin.

2 | 2. Geologic and Oceanographic Setting

2.1 | Geologic Context

The Great South Basin (GSB), positioned on the southeastern margin of New Zealand's South Island, covers approximately 100,000 km^2 in area (Figure 1). Its depth ranges from 100 m at the shelf edge to >2500 m on the lower slope, with sediment fill reaching up to 8.6 km and spanning from the Mid-Cretaceous to the Quaternary (Bostock et al. 2019; Carter, Fulthorpe, et al. 2014; Sahoo et al. 2014). Originating along the eastern margin of Gondwana, the GSB's formation was driven by continental extension that marked the structural separation of the Australian, Antarctic, and Zealandian plates (Eagles et al. 2004; Mortimer 2004; Mortimer 2020; Strogen et al. 2023).

The basin's complex basement, formed from back-arc volcanism and NW–SE-oriented prerift accreted terranes, reflects subduction processes along Gondwana's eastern margin that were active from the Late Paleozoic through the Early Cretaceous (Mortimer et al. 2017). This basement composition, which includes the Torlesse Supergroup composed of schists and metasediments, significantly influenced the structural and depositional evolution of the basin. The GSB has undergone three principal phases of geodynamic evolution: a syn-rift phase, multiple stages of postrift development, and a syn-orogenic phase, each reflecting shifts in the local stress field and plate motions (Bache et al. 2014; Cook et al. 1999; Cox and Sutherland 2007).

The syn-rift phase began in the Mid-Cretaceous (~112 Ma) with the rifting that led to the separation of the Australia, Pacific, and Antarctica plates, resulting in the formation of isolated rift basins characterized by SW–NE- and WSW–ENE-oriented en-echelon half-graben and horst block systems (Mortimer et al. 2017; Sahoo et al. 2020). This rifting continued until the Late Cretaceous (~83 Ma), eventually forming connected depocenters filled initially with alluvial, fluvial, lacustrine, and deltaic sediments, and later by fluvial, estuarine, deltaic, and shallow marine deposits during a major Santonian drowning event (Sahoo et al. 2022 and refrences therein).

From the Late Cretaceous, the postrift phase involved thermal subsidence influenced by active basement faults inherited from the rifting phase. As a result, the GSB was structured into three domains: the Central sub-basin, the Maitai Trough, and the eastern margin, each experiencing variable subsidence rates until the Early Miocene (~19 Ma). High thermal subsidence in the Central sub-basin led to sagging facilitated by local rift shoulders and tilting. Subsidence in the Maitai Trough was comparatively less but evolved from the Oligocene onward due to slope instabilities

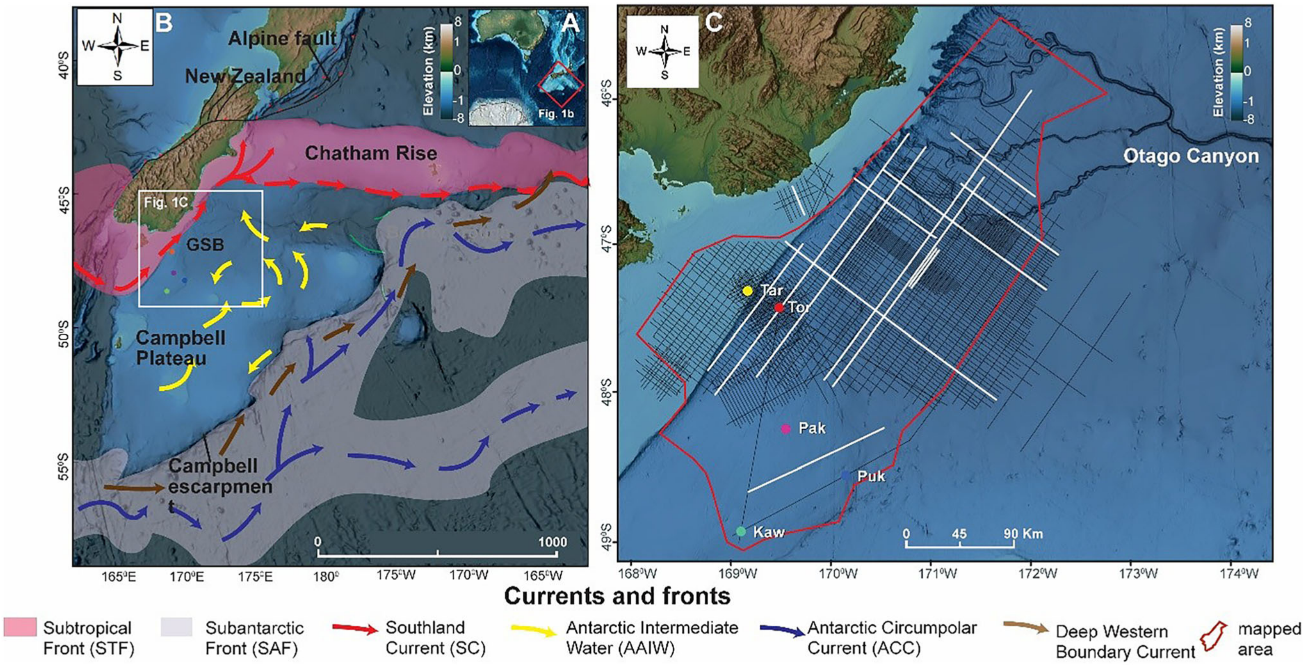

FIGURE 1 | (A) Bathymetric map of the GSB, offshore southeast New Zealand, showing the main dataset used for this study, including seismic profiles and exploration wells. Seismic lines used for figures are highlighted, including line numbers and figure numbers in brackets. Inset figure (B) shows the present-day oceanographic setting in the region.

triggering detachments and sediment deposition shifts (Constable et al. 2013 and refrences therein). Depositional sequences during this phase ranged from transgressive sediments at the end of rifting to lowstand deltas, slope channels, basin floor fans, and finally widespread calcareous sediments due to sediment starvation (Cook et al. 1999).

From the Mid-Miocene (~15 Ma) to the present, the syn-orogenic phase was characterized by selective transpression along inherited syn-rift faults. The uplift associated with movement along the Alpine Fault led to the development of anticlinal structures and influenced sedimentation patterns. This phase's depositional sequence included calcareous sediments in the central and eastern parts, with shelf-margin clastic wedges along the western margin (Cook et al. 1999).

This study focuses on the sedimentary sections from the Middle Eocene to the Quaternary, including the Laing Formation (calcareous shales and argillaceous limestones), the Tucker Cove Formation (siliceous limestone), the Penrod Formation (argillaceous, cherty limestone), and overlying Neogene to Quaternary deposits (Figure 2). Collectively, these units encapsulate a range of pelagic to hemipelagic processes as well as sediment gravity flows and contourites, spanning environments from the shelf to the continental slope and reflecting dynamic deposition from the Eocene to Recent periods.

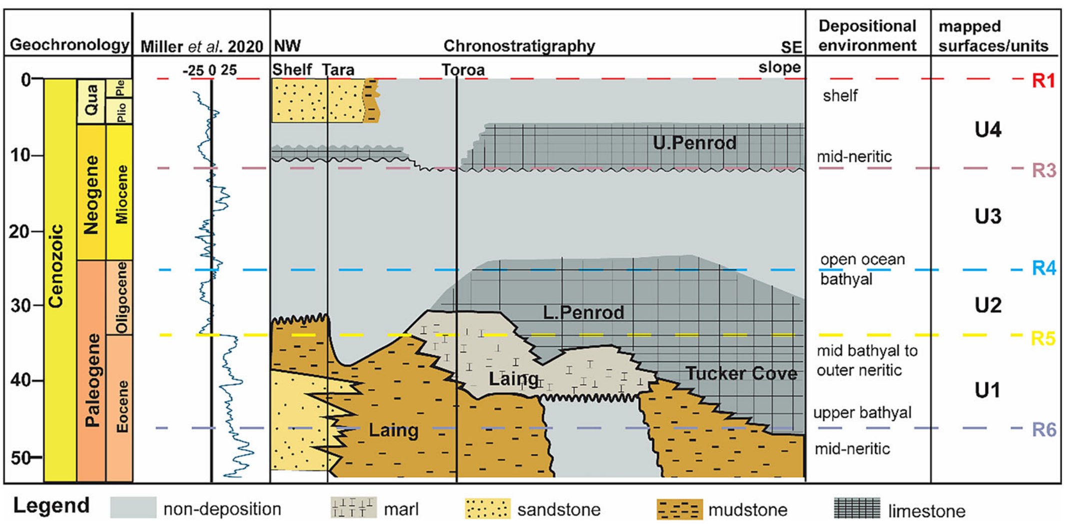

FIGURE 2 | Stratigraphic chart of the GSB, modified from (Cook et al. 1999). The dashed lines refer to the seismic stratigraphic surfaces interpreted in this work. Smoothed sea-level curve from (Miller et al. 2020). Mapped seismic surfaces and units are from this study.

2.2 | Oceanographic Context

The oceanographic dynamics off the southeast South Island of New Zealand are primarily influenced by the interaction between the Subtropical Front (STF) and the Southland Current (SC), alongside upwelling from intermediate-depth waters (Figure 1). Specifically, the STF and the SC are within approximately the upper 200 m. The SC often energizes the upper few hundred meters locally to about 500–600 m, and the nearby Subantarctic Front (SAF) occupies shallow to intermediate depths from the surface down to 1200 m (Chiswell et al. 2021; Stevens et al. 2021). The STF delineates the cooler, fresher subantarctic waters from the warmer, saline subtropical waters, creating pronounced temperature and salinity gradients (Sutton 2001). This front supports the northeastward-flowing SC, which is bathymetrically constrained along the shelf-edge and upper slope, with a flow rate of 8.3 Sv predominantly composed of Subantarctic Water (Sutton 2003). The regional oceanography is also shaped by the submerged Campbell Plateau, which serves as a topographic barrier influencing water mass distribution and the hydrodynamic regime across the GSB and adjacent areas (Hadfield et al. 2007; Sutton 2001; Weaver et al. 1998). Constrained to deeper waters, the Deep Western Boundary Current and the ACC flow in a broadly east to northeastward direction to the south of the study area (Chiswell et al. 2021; Sokolov and Rintoul 2009).

2.3 | Physiography

The principal physiographic domains in the GSB are the continental shelf, slope, and rise (Figure 1). A large and relatively flat continental shelf trends N–S from the coastline to 150 m water depth, with an average slope of 0.8° in the southwestern and central sectors and up to 1.7° in the northeastern region. It exhibits a variable width, wider in the SW area at around 60 km, narrowing to 30–40 km in the central area and to 20–30 km in the NE area (Carter et al. 1985; Chiswell et al. 2021).

Several structural highs, such as the Tūātara Volcanic complex, Tākapu High, Toroa inverted anticline, and Tara High, occur between 46° and 47°S latitude. These structural features can be grouped into two categories. The Late Cretaceous to Early Eocene geological features align with WNW–ESE structural domains, reflecting the orientation of the underlying Paleozoic basement structures inherited from earlier tectonic events (Phillips and Magee 2020). In contrast, the Oligocene to Miocene topographic highs are associated with localized dextral strike-slip movements that exploited NW-oriented zones of weakness in the surrounding basement rocks (Carter 1988). These structural highs have created depocenters, which are considered mini sub-basins (Carter 1988; Cook et al. 1999).

The shelf edge is located at a depth of around 150 m and exhibits a rugged, arcuate morphology. The continental slope is located between 150 and 2500 m depth below sea level (m SSL). The upper slope has a gradient of 2°–4°, situated between 150 and 500 m SSL with an average width of ca. 8 km. The middle slope, from 500 to 1000 m SSL, is narrow in the northern part of the region (10–30 km) with a gradient of to 0.8° and broadens into an extensive very low-gradient (<0.2°) area in the south up to 150 km wide, known as the Southland Terrace. The smooth lower slope is located between 1000 and ≥2500 m water depth. The slope is cut by a series of downslope channels in the north and an alongslope-oriented moat in the south.

3 | Data and Methods

3.1 | Dataset

The data used in this study have been obtained from the New Zealand Petroleum and Minerals (NZMP) authority and from the National Institute of Water and Atmospheric Research (NIWA). The seismic reflection data consist of several old surveys and recently reprocessed data with different vintage quality. Single and multibeam bathymetric data from NIWA and reports from wells used (Kawau, Toroa, Tara, Pakahā, and Pūkaki) in the integration contained check shot information, logs, and formation tops (Hunt International Petroleum 1977a, 1977b, 1977c, 1978; Placid Oil 1984).

This study used five 2D poststack time-migrated (PSTM) datasets obtained from the 2016 New Zealand Petroleum Exploration Data Pack (New Zealand's Minerals and Petroleum Industry 2016), which are summarized with their acquisition parameters in Table S1. These datasets are all located in the South Island covering the entire SE offshore GSB (Figure 1). They were obtained as exploration surveys and are characterized by moderate vertical and horizontal resolution. The seismic surveys were processed to zero phase with SEG normal polarity, according to the European polarity convention.

Hydrographic data comprised high-resolution salinity cross-sections created in Ocean Data View 4.0 to illustrate the distribution of the main water masses throughout the GSB (Figure S1). These cross-sections were also used to identify vertical or lateral changes in the water masses, in particular for salinity and temperature. These were overlain with seismic data, taking into account the different domains (time vs. depth) to allow visual comparison of oceanographic and morphosedimentary features (Schlitzer 2011).

3.2 | Methodology

This study mapped the Mid-Eocene to Holocene succession. The main discontinuities were constrained by well data and previous chronostratigraphic studies (see Table S2; Constable and Crookbain 2011; Cook et al. 1999). Well-to-seismic ties were carried out using checkshot data from the Toroa and Tara wells (Figure S2), which provided a direct shelf to slope correlation, and further refined by creating synthetic seismograms. The key horizons or bounding surfaces identified are: R6 (T50, which corresponds to ~45 Ma), R5 (T70, ~33.7 Ma), R4 (T80, ~27 Ma), R3 (T90, ~12 Ma), R2 (T100, ~12 Ma), and R1 (seafloor, 0 Ma). The "T" notation is their equivalence to those identified in previous studies (Constable et al. 2013; Strogen 2014) and is used to mark project specific seismic sequence boundaries whose ages were constrained by well ties and chronostratigraphic calibrations. They are identified through their geometrical relationships with the underlying and overlying strata, and characterized either by the reflection terminations observed at the boundaries or by the contrasting seismic facies between the adjacent strata above and below the surface (Embry 2009). The seismic units and bounding surfaces are shown in the regional line interpretation

(Figure S2). Seismic time maps were converted to approximate depth thicknesses following the procedure of Cook et al. (1999) utilizing the equation where $\text{Depth} = -21 + 1.48\text{TW} + 1.80648(\text{TR–TW}) + 0.0008347(\text{TR–TW})^2$. Here, TR represents the one-way travel time (ms) to the reflector and TW is the one-way travel time (ms) to the seafloor.

Isochron maps were created to identify major depocenters and sedimentary routing pathways between the outer shelf/upper slope and the deep basin. Analysis of the seismic facies (Figure S3), which changed both laterally and vertically through time, served as the foundation for the creation of morphosedimentary maps.

4 | Results

The results are presented in two parts: first, the seismic stratigraphic analysis (Section 4.1) and second, the morphological and depositional elements observed within those units (Section 4.2). Brief interpretations are provided as required.

4.1 | Seismic Stratigraphic Analysis

Bounding surfaces R1–R6 are used to define four primary seismic units (U1–U4) and two subunits (U4A and U4B) (Table S3 and Figures 3–7). Based on well ties and correlation with previous studies, the succession ranges from Mid-Eocene to Recent, where R1 is the seafloor. The subdivision of U4 into U4A and U4B is on the basis of significant stratal terminations exhibited along different portions of the physiographic domains.

4.1.1 | Seismic Unit 1: Mid- to Late Eocene

Seismic Unit 1 (U1) is bounded by seismic horizons R6 and R5 (Figures 3–7 and Table S3). The basal reflection R6 is defined by a marked change in acoustic facies (Figures 3 and 4). This surface has been dated as Middle Eocene, at approximately 45 Ma (Constable et al. 2013), and marks the Early to Middle Eocene boundary. It has been previously named discontinuity T50 (Constable and Crookbain 2011; Constable et al. 2013). This horizon is characterized by a moderate-amplitude reflection that has a smooth surface, locally cut on the middle slope by concave-up depressions, which we interpret as channel-like erosive features. Several structural highs were already developed by this time (Figure 3A,B), which can be clearly observed on the isochore (time thickness) map of R6 (Figures 8 and 9).

The seismic character of U1 varies across the various physiographic domains of the margin (Figures 3–7). Beneath the shelf, U1 is characterized by moderate-amplitude parallel, continuous reflections, more rarely chaotic, that thin northwestward and locally onlap a Miocene structural high, the Tākapu High (Figure 3A). In the far northwest, about 60 km landward from the shelf edge (Figure 3A), this unit also shows onlap and toplap geometries, where reflections terminate against overlying reflections. At the shelf edge (Figure 3B), its section steepens into prominent sigmoid reflections, and on the upper slope (Figure 3B), its reflections dip and diverge with local downlap and onlap against a broad domal structural high with gentle flanks. Below the middle slope, U1 is approximately 600–700 m thick. It shows a vertical change in reflection configuration from low-amplitude parallel to subparallel continuous reflections upward into variable amplitude discontinuous to chaotic reflections (Figure 3B). The unit is capped by high-amplitude laterally extensive reflections that exhibit toplap truncation against the overlying R5 surface. In places, several reflections are truncated by the overlying R5 surface and form concave-up geometries (Figure 4B–D). Downlap terminations occur mostly along the SE flank, at the base of U1 (e.g., Figure 3B,E).

Many faults have been identified in U1 (Figures 3B and 4B). The faults do not reach the seafloor, lacking any organized large-scale fault orientation and are localized within the unit along the middle slope. This fault system comprises several layer-bound arrays of closely spaced small normal faults with small offsets in the seismic reflections (Figures 3B, 4B, and 5B). Below the lower slope, U1 is characterized by high-amplitude, high-frequency, laterally continuous concordant reflections (Figures 5 and 6). This unit is approximately 370 m thick on the lower slope.

The isochron map of U1 shows thicknesses up to 350 m below the middle slope in the northern region and as much as 750 m in the south (Figure 9). Areas with reduced thicknesses appear to follow downslope channels, and therefore signify sediment erosion or nondeposition.

4.1.2 | Seismic Unit 2: Early to Late Oligocene

Seismic Unit 2 (U2) is bounded by seismic horizons R5 and R4. R5 corresponds to a discontinuity at the Eocene–Oligocene boundary of ~33.7 Ma and has been previously identified as the T70 discontinuity (Constable and Crookbain 2011) and labeled as the TE discontinuity in other studies (Sarkar et al. 2019). It is characterized by a high-amplitude reflection (HAR) and exhibits concordant and discordant relationships with U1 (Figures 4 and 6). Reflection R5 also exhibits incised, erosional surfaces with HARs along its base (Figure 4B,C).

Moderate-amplitude, parallel to wavy continuous reflections are the defining feature of U2 (Figures 4–7). Internally, this unit consists of vertically stacked alternating sequences of moderate- to low-amplitude seismic facies. U2 has been partially eroded and is completely absent in the WNW (Figures 3 and 9). Along the continental shelf, U2 is characterized by thin, laterally continuous, parallel to divergent reflections, commonly disrupted by evenly spaced normal faults. This unit onlaps the underlying discontinuity R5. Across the upper slope U2 is particularly thin, consisting of moderate-amplitude, continuous, parallel and divergent reflections, whereas across the middle slope, the thickness is highly variable. This unit exhibits its greatest thickness ≥ 350 m across depressions along the underlying surface, which were filled during its deposition (Figure 9). Within these depressions, U2 is characterized by stacks of low-amplitude, discontinuous, subparallel to parallel and divergent aggrading reflections, which infill a concave-upward basal boundary R5 (Figure 4).

The isochron map of U2 (Figure 9) shows thinner sediment across the southwest and northwest areas of the shelf. The main depocenters, up to 350 m in the middle slope, are located in areas (Figure 9) that were previously eroded and subsequently infilled during the development of U2.

4.1.3 | Seismic Unit 3: Late Oligocene to Mid-Miocene

The Late Oligocene to Mid-Miocene succession (~27–12 Ma), deposited between the R4 discontinuity at the base and the R3

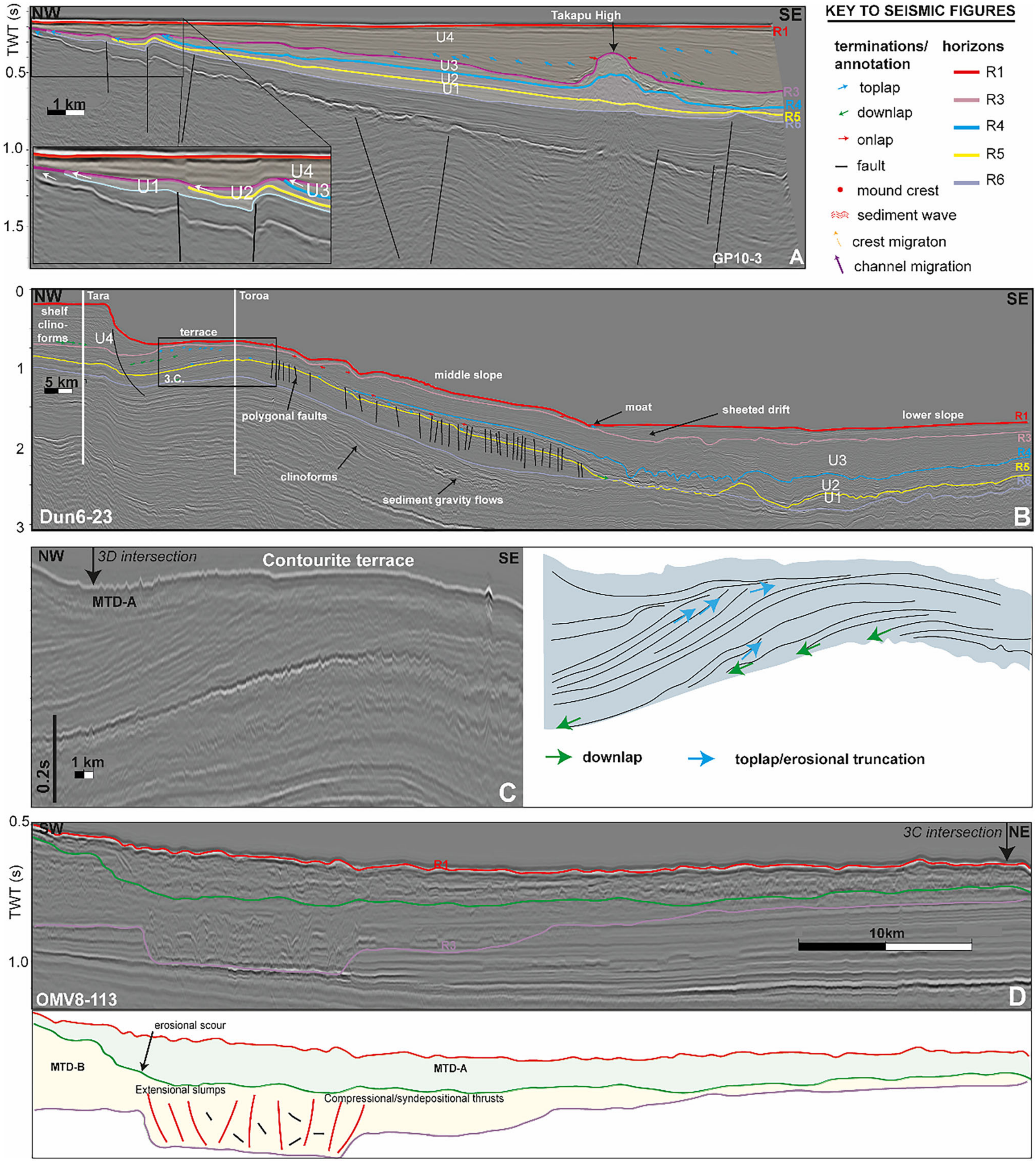

FIGURE 3 | Interpreted seismic lines extending from the shelf, across the continental slope and into deep water. Seismic line locations are shown in Figure 1. (A) Shelf profile showing thinning to the NW and onlap onto a Miocene structural feature, the Takapu High. (B) Seismic profile intersecting two deep exploration wells, from the shelf to deepwater. Note the steep shelf margin with prominent clinoforms, inboard of a prominent contourite terrace. (C) Seismic profile and line sketch of the contourite terrace, with the U3 sequence exposed at the seabed. (D) MTC located between the slope break and contourite terrace, indicating repeated mass failure of the upper slope, possibly due to the combination of high sedimentation rates and bottom-current erosion.

discontinuity at the top, is defined by seismic Unit 3 (U3). The underlying discontinuity R4 has been dated as Late Oligocene (~27 Ma) and labeled as T80 in previous studies (Constable and Crookbain 2011). Its acoustic character is highly variable. It is primarily distinguished by parallel reflections of moderate amplitude, though HARs are occasionally seen (Figures 4B,C and 5B). The reflections against the R4 discontinuity downlap or onlap and range in amplitude from moderate to high across the shelf (Figure 3A).

Subhorizontal, parallel, continuous, moderate to high-amplitude reflections are the hallmark of U3 (Figures 4–7). It exhibits both concordant and discordant relationships

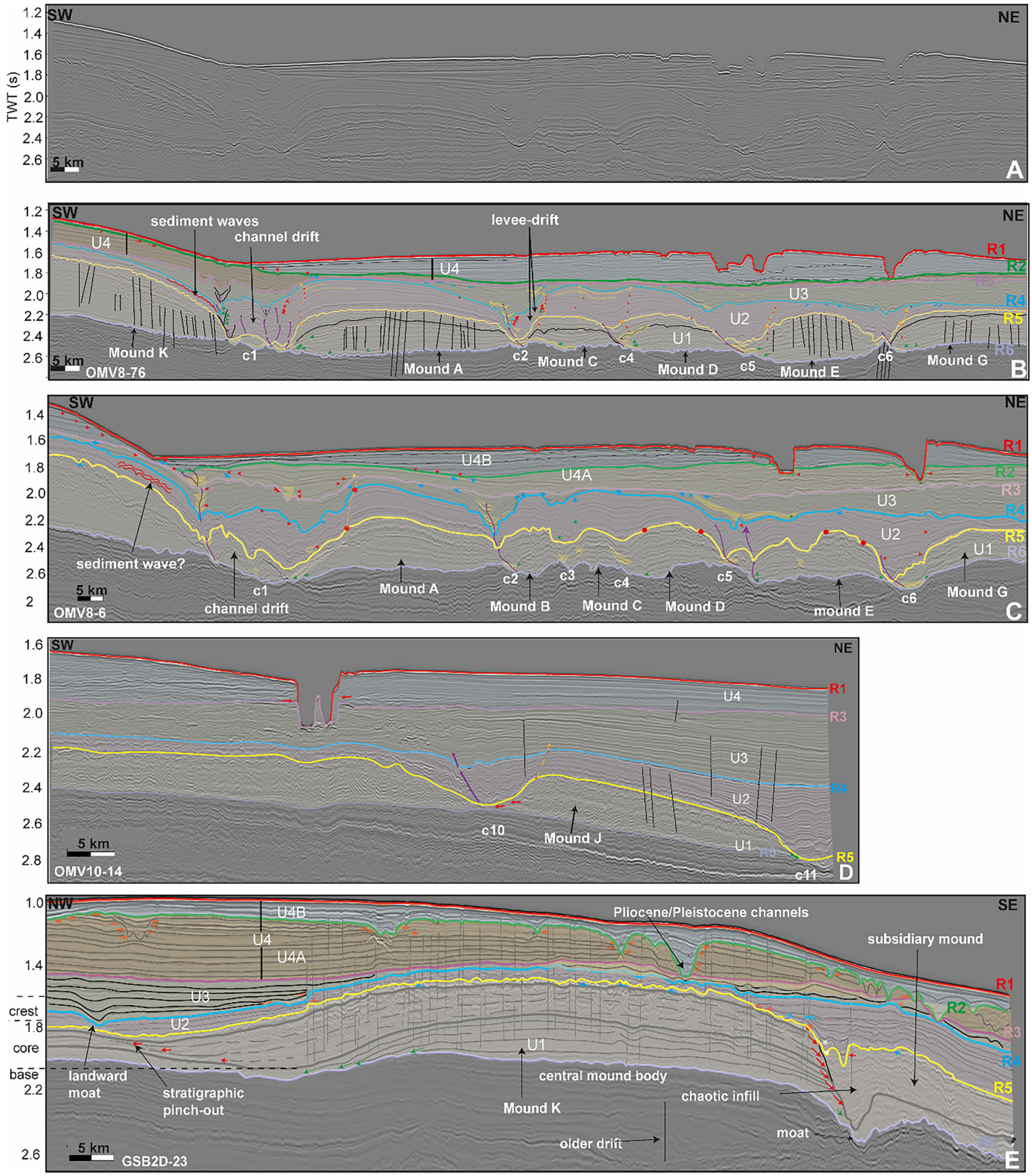

FIGURE 4 | Seismic profiles across the middle slope (water depth ~750–1400 m) displaying the erosional and depositional features of the mixed depositional system, primary seismic units (U1–U4), discontinuities (R6 to R1) and the system's ultimate burial in the Oligocene. Line locations are shown in Figure 1.

with its bounding discontinuities. Local toplap and downlap truncations are identified in certain sectors across the margin. Across the upper slope, U3 presents variable thickness, mainly due to incision of the R2 and R1 surfaces against the underlying discontinuity R3. Its thickness tends to increase basinward, and it thins toward the middle slope (Figure 6).

The isochron map of U3 reveals that the shelf area in the west is particularly thin or absent (Figure 9). Toward the upper and middle slope, the sediment thickness is up to 50 m on average, whereas local depressions and lens-shaped reflection packages (Figures 4B,C and 5B) contain moderate sediment thicknesses up to 100 m. U3 thickens to the northeast and southeast below the lower slope, locally reaching ~450–500 m (Figure 9).

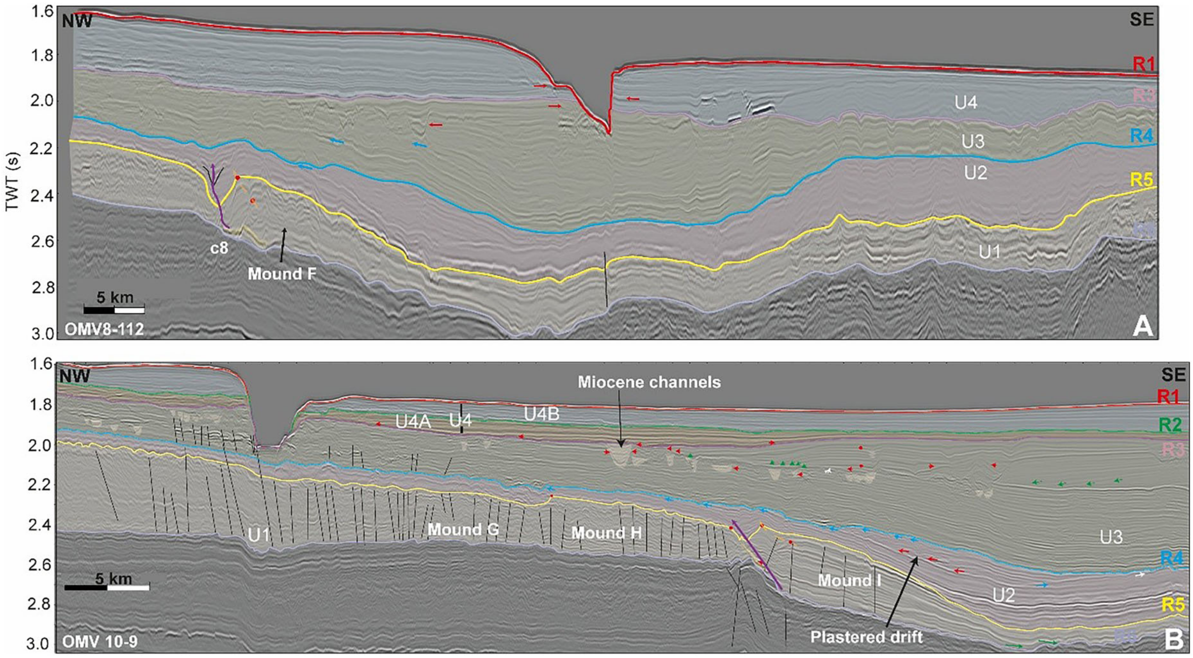

FIGURE 5 | Interpreted seismic lines across the middle continental slope in the northern part of the basin, displaying the erosional and depositional features of the mixed depositional system in U1–U4. The sections also show deeply canyon systems incising the U4 and U3 seismic units. See Figure 1 for line locations.

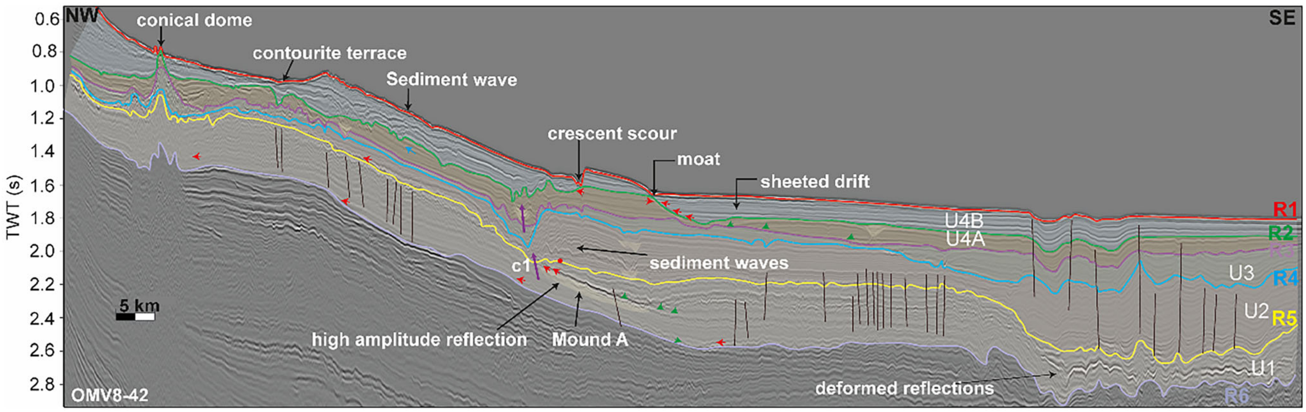

FIGURE 6 | Interpreted seismic lines across the entire shelf to deep basin in the central part of the basin, displaying a range of erosional and depositional features. See Figure 1 for line locations.

4.1.4 | Seismic Unit 4: Mid-Miocene to Recent

Seismic Unit 4 (U4) encompasses the Mid-Miocene to Recent succession (~12–0 Ma), deposited between the R3 basal horizon and the seafloor (Figures 3–7). Horizon R2 subdivides U4 into two subunits (namely, U4A and U4B) (Figure 4E). The R2 discontinuity is characterized by high-amplitude, concave-upward reflections across several parts of the study area (Figures 4E and 6).

The reflection character of U4 is highly variable and difficult to generalize. Across the shelf (~0–150 m), U4 consists of oblique and sigmoid progradational, low- to high-amplitude reflections (Figure 3A,B). Its foresets comprise steeply dipping reflections that transition toward the bottomset and downlap against the underlying R3 discontinuity (at the toe of the upper slope), while the topset truncates against the top R5 discontinuity or becomes conformable across the more proximal parts of the shelf (Figure 3A,B). Along the upper slope (150–500 m), U4 is subdivided into subunit 4A below and subunit 4B above (Figure 6). Subunit 4A consists of low- to moderate-amplitude, chaotic reflections truncating at the flanks of mounds with HAR tops (Figure 6), whereas subunit 4B consists of moderate-amplitude, divergent to oblique reflections truncating against the flanks of the mounds (Figure 6). Along the middle slope (~500–1000 m), sub-unit 4A is dominated by moderate-amplitude, parallel reflections that transition upward into high-amplitude, drape-like reflections infilling and truncating against the sides of several depressions (Figure 4C,E), whereas subunit 4B consists of moderate-amplitude, parallel reflections (Figure 4C,E). On the lower slope (1000–≥2500 m), U4 shows an alternation of moderate to high-amplitude, parallel reflections, commonly truncated by concave-up depressions at the present-day seafloor (R1) (Figures 4–6).

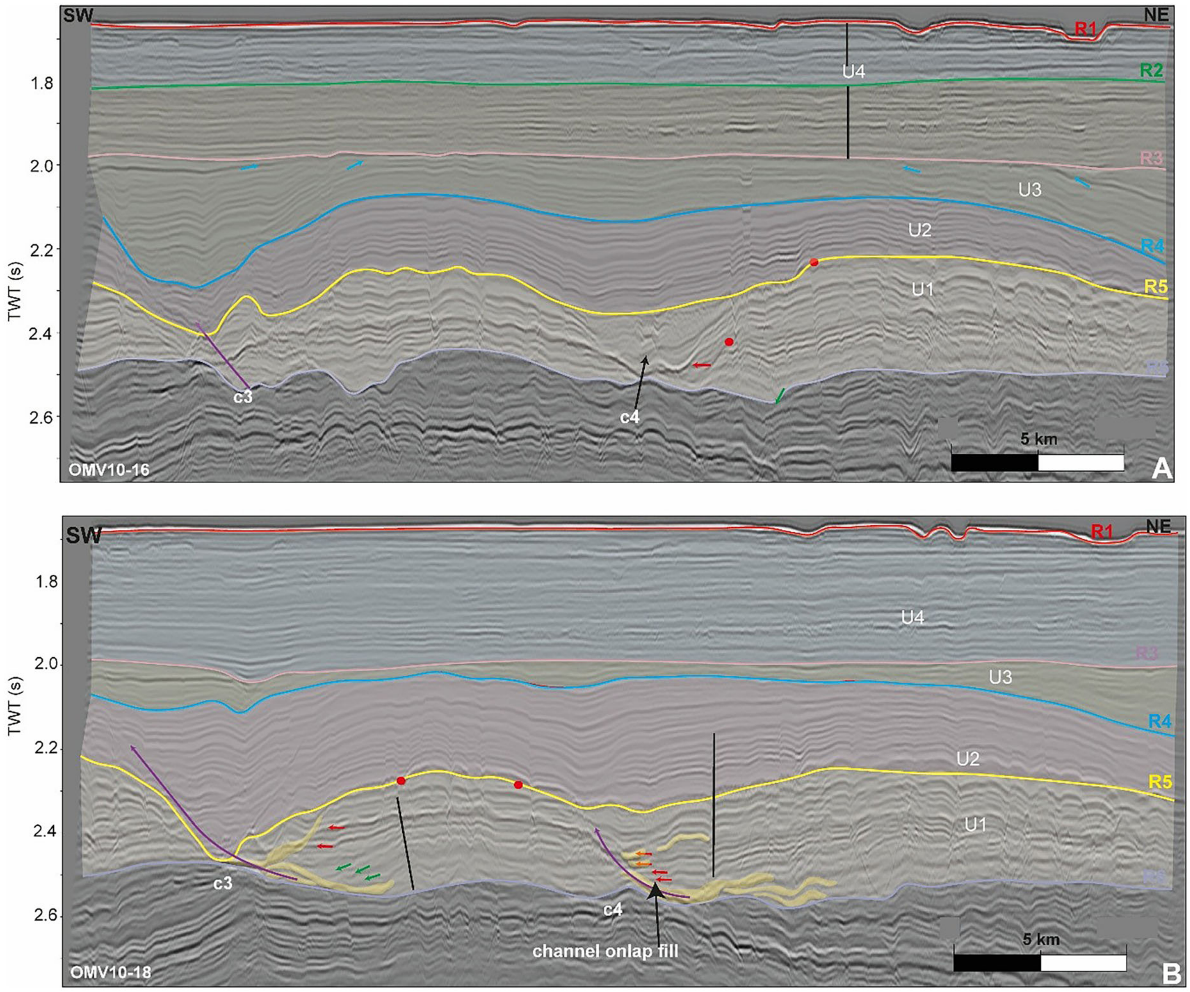

FIGURE 7 | Interpreted seismic lines along the middle continental slope, displaying the primary seismic units (U1–U4), morphological features of the mixed depositional system represented by mounds, channels, and channel-fill deposits. See Figure 1 for line locations.

The isochron map of U4 reveals depocenters around 500–700 m thick in the southern and central (lower slope) sectors (Figure 9), with some indication of an orientation parallel to the bathymetric contours. Along the outer shelf and shelf edge, its thickness reaches ~900 m, while it reduces to ~200 m or less on the upper to middle slope (Figure 9).

4.2 | Morphological Elements: Paleogene

4.2.1 | Nondepositional Elements

A series of concave-up depressions bounded by basal HARs are the primary features occurring within seismic Units 1, 2, and 3 (Figures 4–7). Seismic sections (Figures 4 and 7) show they also contain internal packages of chaotic, discontinuous, or divergent prograding reflections that infill the depressions, with local onlap against their walls (Figure S3G,H). These depressions also display HARs at their base that extend laterally into the adjacent depositional mounds (Figure S3C).

These features are interpreted as NW–SE downslope-oriented channels developed along the continental margin, crossing from the upper (150–500 m) to the lower continental slope (1000–≥2500 m) (Figures 4, 5, and 7). On average, the channels are 25–60 km long, 3–20 km wide, and <300 m deep (Figures 4–9). They emanate from the upper slope as low sinuous channels (~1.05), increasing to ~1.2 across the middle slope (500–1000 m) where several distributaries are observed (Figures 8 and 9). They evolve downslope from relatively narrow V-shaped channels (with aspect ratios of ~1.5–1.8; Figure 4B,C) to broader U-shaped channels (with aspect ratios ~2.1–2.4; Figures 4D and 7), becoming progressively wider and shallower along the lower continental slope (Figures 8 and 9).

In map view (Figures 8 and 9), some channel margins show lateral offsets of ~2–5 km, expressed as overlapping or stepped terraces, particularly across the middle to lower slope. These offsets indicate episodes of lateral migration, mainly toward the southwest although in places individual channel complexes are preferentially offset to the northeast, where they are locally associated with vertical aggradational stacking (Figure 4B,C). These observations demonstrate that the channels are not purely erosional in origin, but instead record mixed erosional and depositional processes.

4.2.2 | Depositional Elements

Eleven prominent elongated mounded sediment bodies are evident within units U1 and U2, mostly along the middle continental slope (500–1000 m) (Figures 4–7). Table 1 summarizes the

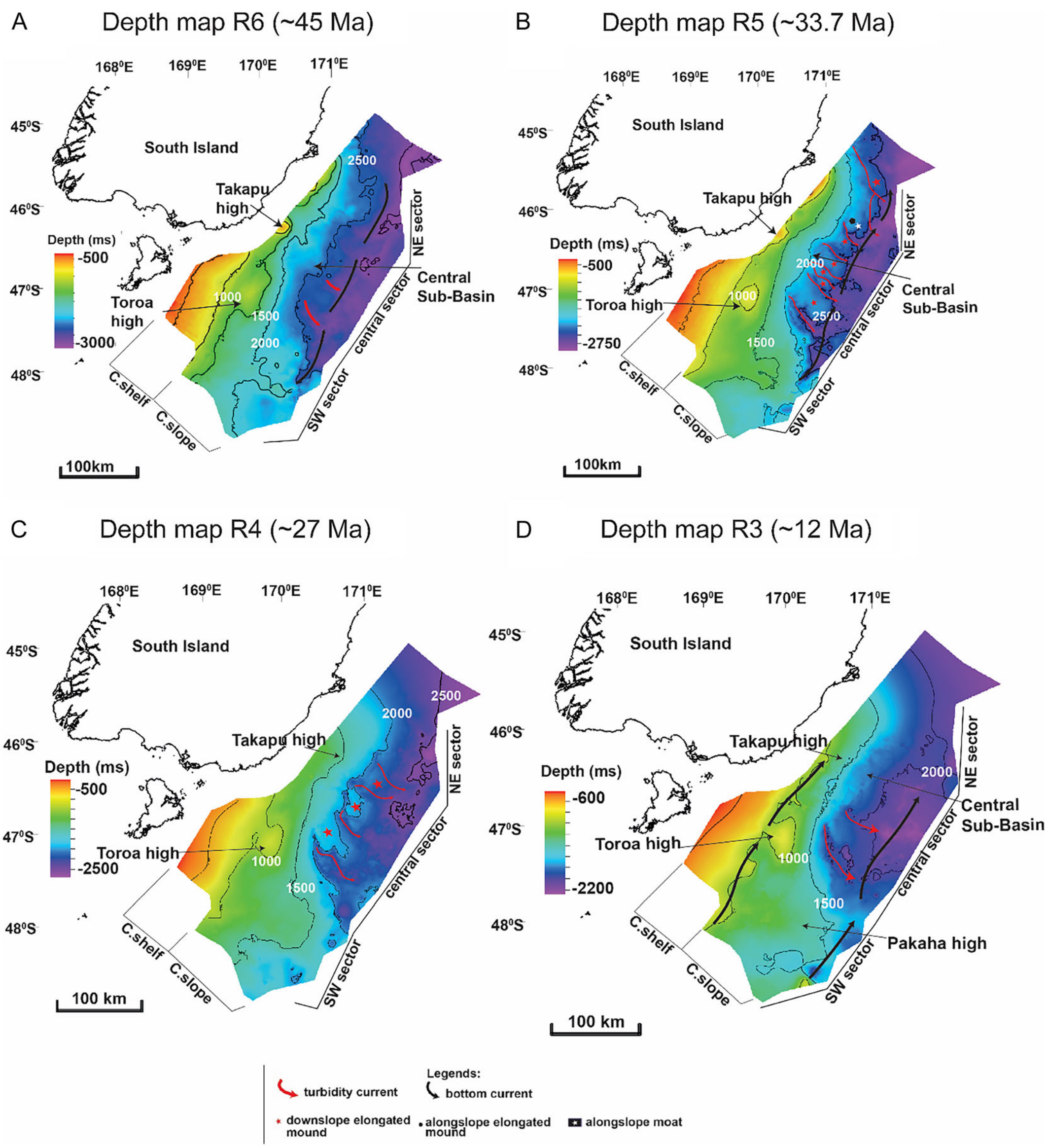

FIGURE 8 | Depth maps of seismic horizons R6-R3, showing the size and scale of buried mounds and channels/moats in the GSB between the Middle Eocene and Middle Miocene.

morphological relationship of these mounded sediment bodies. These mounded features, here designated Mounds A–K, display thicknesses of 350–700 m, widths averaging between 8 and 24 km and lengths of 18–80 km. They are oriented downslope perpendicular to the SW–NE trending continental margin (Figures 8, 9).

Mounds A, F, G, H, I, and J are asymmetric in cross section, distinguished by a smooth, gently dipping north-eastern flank with average slopes of 0.1°–0.8°, and a steeply dipping southwest flank with average slopes of 1°–2°. The crest is closer to the steeper, southwestern flank. Internally, they comprise low- to high-amplitude reflections that alternate in a sub-parallel pattern (Figures 4–7). These mounds are aggradational, exhibiting a subtle migration of crests in a northeastward direction (Figure 4B,C).

Mound K is a larger asymmetric body located toward the SW sector of the middle slope. It covers an area around 4200 km^2, approximately 130 km long, 75 km wide, and 750 m thick (Figure 4E). It has an elongated asymmetric mounded geometry, oriented parallel to the slope, with a gentle smooth side in the southwest direction (0.1°–0.8°) and a steep side in the northeast direction (1°–2°). Mound K is associated with a subsidiary drift approximately 40 km long, 15 km wide, and about 500 m thick (Figure 4E).

Mounds B, C, D, and E are more symmetric in shape, some having double crests that are only slightly elevated (Figure 4B,C). These show migration in a northward direction or oblique to the margin.

There is another broad and slightly mounded body within U2 that is plastered onto and across the lower to middle slope in the southern part of the study area (Figure 5B). This is distinguished by an asymmetrical morphology, smooth flat top, a gently sloping depositional flank to the southeast, and steeper flank to the northwest. It has an average thickness of around 350 m, length over 50 km, and widths up to 25 km. Internally, it has parallel, continuous seismic reflections with moderate to high amplitudes and an overall aggradational pattern (Figure S3E). On its seaward side there are smaller sediment mounds that appear to diverge from the main body.

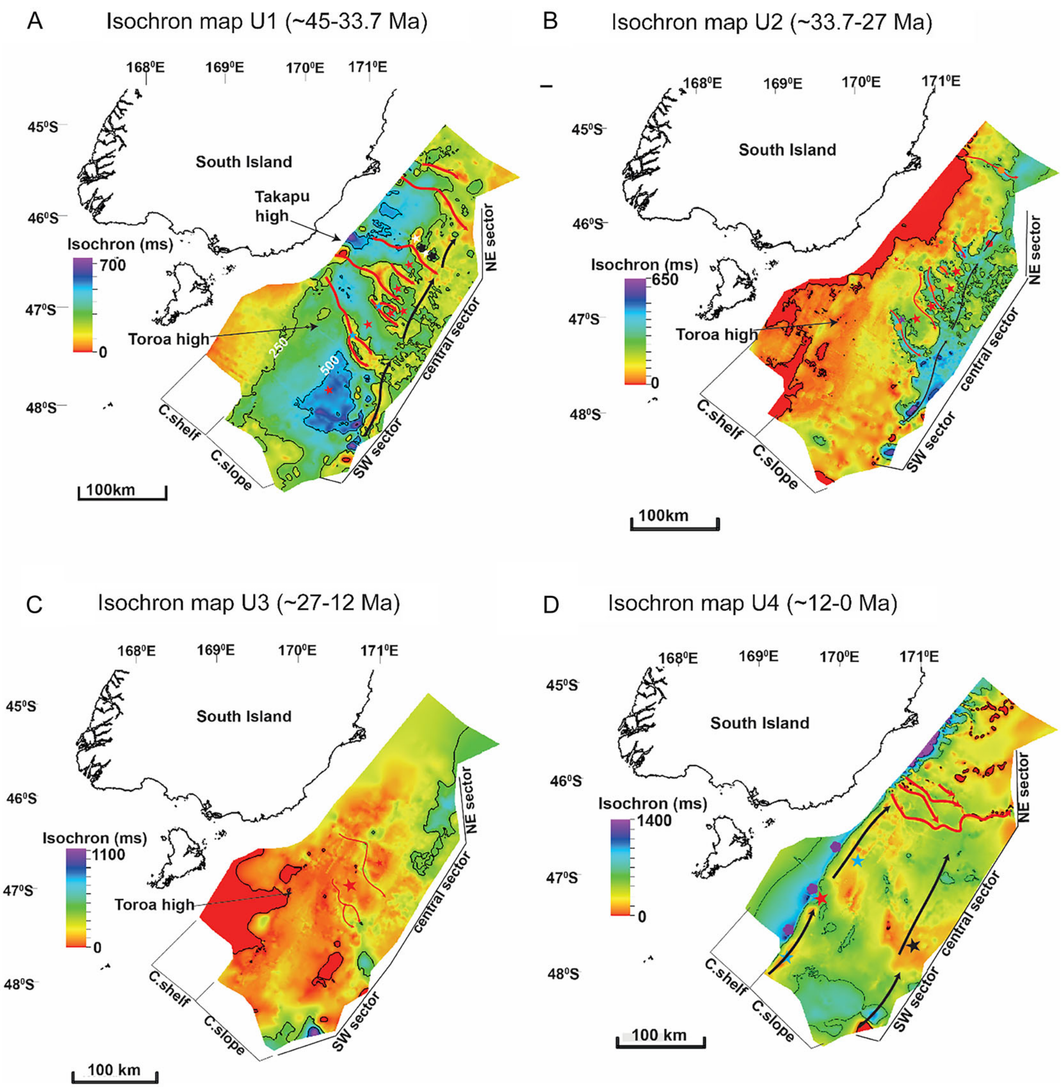

FIGURE 9 | Isochron maps of seismic units U1–U4. Large mounds formed in the Eocene–Oligocene (U1, U2) before being largely buried in the Late Oligocene (U3). A new CDS formed since the Middle Miocene (U4) in association with the development of the Otago Canyon system.

TABLE 1 | Summary of the morphometric character of the mounds.

Mound	Area, km^2	Maximum width	Length	Maximum height, m	Morphology	Orientation to margin
A	1773	24	80	300	Asymmetric	Oblique
B	137	8	19	277	Asymmetric	Oblique
C	296	7.95	43	225	Symmetric	Oblique
D	499.7	16	34	255	Symmetric	Oblique
E	370	17.5	27.7	292.5	Symmetric	Oblique
F	272	14.9	24.5	292.5	Asymmetric	Parallel
G	517	15.1	52	232.5	Asymmetric	Parallel
H	333	16.4	29.6	198	Asymmetric	Parallel
I	151	13	17.8	177.75	Asymmetric	Parallel
J	920.8	24	62	300	Asymmetric	Oblique
K	4200	75	130	500	Asymmetric	Parallel

Seismic profiles show packages of stacked asymmetric wavefields, comprising low- to high-amplitude, aggradational reflections evident within U2 and U3 (e.g., Figures 6 and S3F). This reflection pattern is characterized by a short and thick upslope flank and a thin, longer downslope flank. Wave heights are on average <15 m high and 1–2 km long, and the wave fields consist of 6–8 rows of waves (Figure S3F). These features, interpreted as sediment waves, occur within the elongated mounds and appear to be oriented oblique to the downslope elongation of the mounds.

4.3 | Morphological Elements: Neogene to Recent

4.3.1 | Nondepositional Elements

Four main channel complexes cut across the continental slope in the eastern sector of the GSB (Figure 10). These are designated as submarine canyons in the literature (Mitchell 2012), so we continue to use this terminology. From west to east, they include the South Molyneux Canyon (SMC), North Molyneux Canyon (NMC), South Brodie Canyon (SBC), and North Brodie Canyon (NBC). Each canyon possesses a head region characterized by a narrow, elongated headward scarp displaying fused scars, from which the canyon initiates as a V-shaped feature with several tributaries that emanate from the upper slope (Figure 11). Notably, the heads of the SMC and NBC extend across the shelf edge, whereas the NMC and SBC remain confined to the slope (Figure 11).

Across the upper slope, these canyons exhibit gradients of 7°–14° (Figure 11). The gradient decreases rapidly into the middle (3°–5°) and lower slope (1°–2°) regions (Table 2), where the channels ultimately merge as tributaries to the Bounty Channel (Figure 10B). Their lengths vary between 67 and 78 km, and their depths range from 150 to 380 m. They are typically 1–3 km across but widen to as much as 10 km where they merge into the submarine Bounty Channel (Figure 10B). Overall, the canyons display straight (1.02–1.04) to moderately sinuous (1.08–1.19) pathways throughout their course. A summary of their morphometric characteristics is provided in Table 2.

The present-day submarine canyons have discontinuous HARs along their axes (Figure 11). Within the slope succession of U4 (and in between channels), there are channels at the surface, buried channels, channel terraces, and scars along canyon walls (Figure 11). The infill of the buried channels is characterized by chaotic to discontinuous high- to low-amplitude seismic reflections (Figure 11A,B). These buried channels are interpreted as paleo-channels, while the inactive surface channels are regarded as abandoned (Figure 11B). Drape-like facies filling them suggest episodic infill. Terraces are identified as step-like, flat structures with low- to moderate-amplitude reflections (Figure 11A), while scars disrupt reflection continuity and occur adjacent to faults in canyon walls (Figure 11D). Terraces are interpreted as channel-margin features linked to canyon development, and the canyon wall scars are consistent with slope failure associated with faulting. In most cases, the canyons appear to have consistently migrated southwestward over time (Figures 4 and 5).

4.3.2 | Depositional Elements

Wedge-shaped reflection packages, thinning progressively away from the channel axis (Figure 11), are prominent morphological

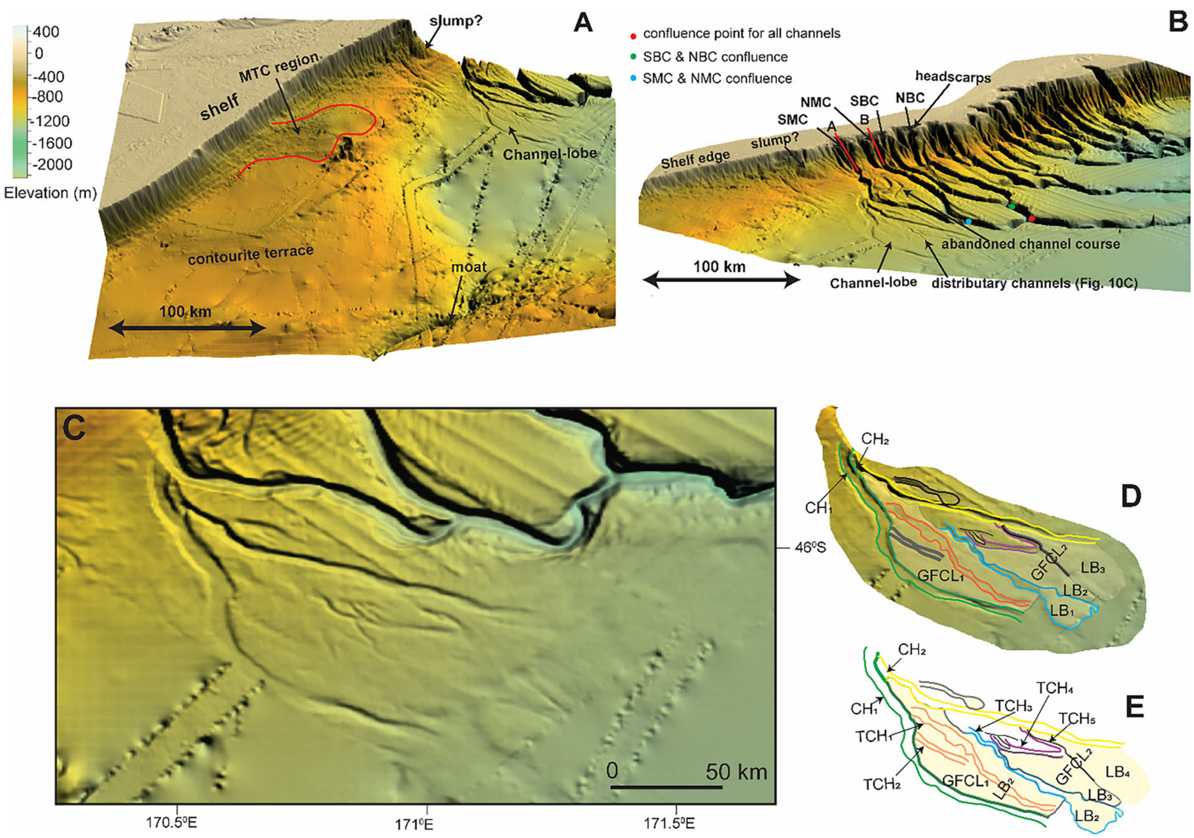

FIGURE 10 | 3D shaded relief of the study area revealing: (A) contourite terrace, MTC and an alongslope moat in the southwest sector; and (B) the four main canyons, channel-lobe sector, and possible slumps in the northeast. (C) zoomed-in image of the bathymetric map in B revealing the distributive channel-lobe system at the southern end of the SBC canyon. (D,E) a schematic interpretation of C identifying the main channels (CH1 and CH2) and their various distributaries (TCH1–5) and the main lobes (GFCL1 and GFCL2) and their various depositional lobes (LB1–4).

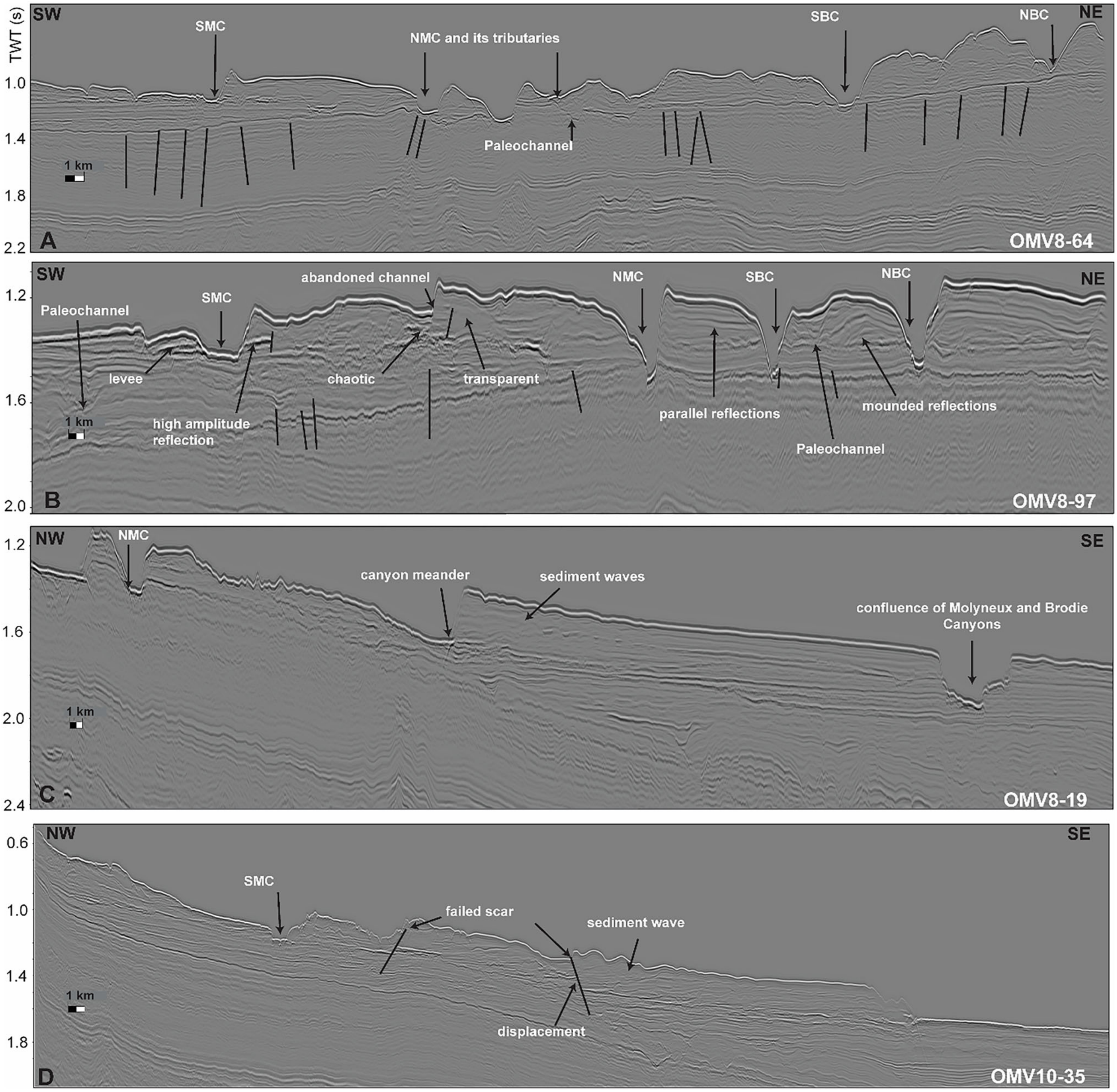

FIGURE 11 | Seismic profiles across submarine canyons in the northern GSB: (A) seismic line SW to NE across the canyons revealing the various tributaries; (B) seismic line SW to NE across the canyons revealing key reflection patterns in the channel axis and interchannel areas, and prominent features such as terraces, failed scars and channel migration; and (C,D) seismic features of the NMC and SMC, showing sediment waves developed at their eastern flank.

elements flanking the submarine canyons and forming on both sides of the channels but with a marked asymmetry in relief, and varied reflection character. In some areas, moderate-amplitude, parallel to subparallel reflections onlap against the canyon walls, while in other locations, discontinuous reflections become offset by faulting (Figure 11B). Furthermore, mounded seismic geometries with concave, moderate-amplitude divergent reflections and zones of chaotic to transparent reflections are also observed (Figure 11B).

These packages are interpreted as channel levees, typically ~20 km wide and ~100 m thick (Figures 10B and 11). The eastern levees typically exhibit greater elevation (~40–60 m) than the western levees (Figure 11B). Levee crests display two distinct forms: smooth, constructional crests or degraded, rugose crests. The crests are commonly tapered, with pointed edges that slope outward over several kilometers from the channel axis (Figure 11B).

Asymmetric wavy reflections, ranging in height from 10 to 30 m and in wavelength from 1 to 3 km, are common on the overbank areas of the levees (Figure 11C,D). These reflections form well-developed packages on the eastern levees, creating trains of undulations that exhibit a downslope decrease in both wavelength and wave height. Their seismic reflections are characterized by undulating, moderately to highly continuous reflections with moderate to high amplitude (Figure 11C,D).

TABLE 2 | Main morphometric characteristics of canyon in the GSB.

Submarine canyon	South Molyneux Canyon	North Molyneux Canyon	South Brodie Canyon	North Brodie Canyon
Total length, km	78.3	73	67.5	69
Canyon indenting style	Shelf indenting	Slope confined	Slope confined	Shelf indenting
No. of tributaries	3	2	2	3
Min–max water depth, m	124–1252	242–1252	202–1392	166–1392
Max incision, m	200	380	220	250
Max width, km	~9	~8	~7	~7
Upper slope gradient, °	14	11.2	8	8.8
Middle slope gradient, °	3°–5°	3°–5°	3°–5°	3°–5°
Lower slope gradient, °	1°–2°	1°–2°	1°–2°	1°–2°
Average sinuosity	1.15	1.13	1.12	1.15

These features are interpreted as sediment waves, exhibiting upslope migration marked by an increasing asymmetry and aggradational patterns higher in the stratigraphic section, near the channel axis (Figure 11C,D). The thickness of sediment wave packets gradually decreases toward the downslope flank, several kilometers away from the channel axis.

Lobe-like features, designated GFCL1 and GFCL2, are situated between two principal channel networks (CH1 and CH2) on the middle slope (500–1500 m) (Figure 10C–E). Bathymetric data indicate that GFCL1 and GFCL2 each comprise multiple stacked lobes and numerous channel-like features (Figure 10D,E). Specifically, GFCL1 consists of a single lobe (LB1), whereas GFCL2 encompasses three lobes (LB2, LB3, and LB4). These lobes extend 15–16 km in length and measure 8–11 km in width and are separated by five channel features (TCH1–TCH5). CH1 and CH2 measure approximately 45–55 km in length, 10–40 m in depth, and 1–3 km in width (Figure 10C).

GFCL1 and GFCL2 are interpreted as extensive channel–lobe systems. The stacked lobes are considered depositional in origin, and the channel-like features are interpreted as distributary channels in planform. The principal channels (CH1 and CH2) likely represent an older, abandoned course of the South Molyneux Canyon and appear to have originated from a single-entry point on the middle slope (Figure 10B–E).

A large chaotic feature is identified within the stratigraphically younger unit of SU4 (Figure 3D), along the upper slope (500–750 m; Figures 10D and 12D), and subdivided into two main bodies, MTD-A and MTD-B. MTD-A is characterized by high-amplitude, chaotic, and discontinuous reflections (Figure 3D). It is bounded at the top by the R1 reflection surface and at its base by a potential erosional surface defined as R2 (Figure 3D). A potential scour, identified by a steeply inclined erosional surface, separates MTD-A from the underlying MTD-B. The thickness of MTD-A varies from about 120 m where the scour is identified and thins toward the NE (Figure 3D).

MTD-B is characterized by chaotic HARs, commonly disrupted by faults, while away from these faulted zones the reflections tend to be discontinuous with low to moderate amplitudes (Figure 3D). It lies beneath MTD-B and is bounded at the top by the R2 reflection and at the base by an irregular surface (reflection R3; Figure 3D).

These two bodies are herein interpreted as a mass transport complex (MTC). The localized areas of disruption within MTD-B are interpreted as syndepositional thrusts.

4.3.3 | Composite Elements

A broad, relatively flat feature occurs in SU4 (Figures 3B,C and 6) along the middle slope of the southern region, at a depth of 550–900 m SSL (Figure 10D). Its seismic reflection character varies across the slope (Figure 3B,C). Toward the southwest, it comprises aggradational, parallel, moderate-amplitude reflections, which are mostly conformable along the southeast and downlap against older surfaces in the west. Locally, on the toe of the upper slope (Figure 3B,C), chaotic and transparent seismic reflections appear to interfere with its conformable reflections. Here, this feature exhibits a convex, slightly folded and deformed seismic facies. Toward the east, its reflections are truncated by undulating concave-up like reflections or onlap and form pinch-out wedges (Figure 3B,C).

These variations in reflection character suggest that this feature shows aspects of both erosion and deposition. This feature is thus interpreted as a gently sloping terrace, with a mean gradient of 0.2°–0.8°, which increases gradually toward the north (Figure 3B,C). Its proximal and distal boundaries are limited by the upper and lower slope scarps, which are characterized by steeper gradients. The terrace widens toward the west and south, where it reaches ~85 km in width, and narrows further northward to around ~30 km upslope of the northeast Canyon. It is partly covered by a large MTC and clusters of conical domes (Figure 6).

Seaward of the terrace on the lower slope, there is an alongslope channel or moat, with a gradient ranging from 2.25° to 2.46°, at water depths of 1000–1250 m (Figures 3B and 6). It has an asymmetric cross section, extending for an average length of ~250 km, with a width of 5–7 km and a depth of 40–60 m, displaying a slightly sinuous morphology. The moat is closely associated with a broad sheeted drift (Figures 3B and 6), reflecting the interplay of erosional and depositional processes.

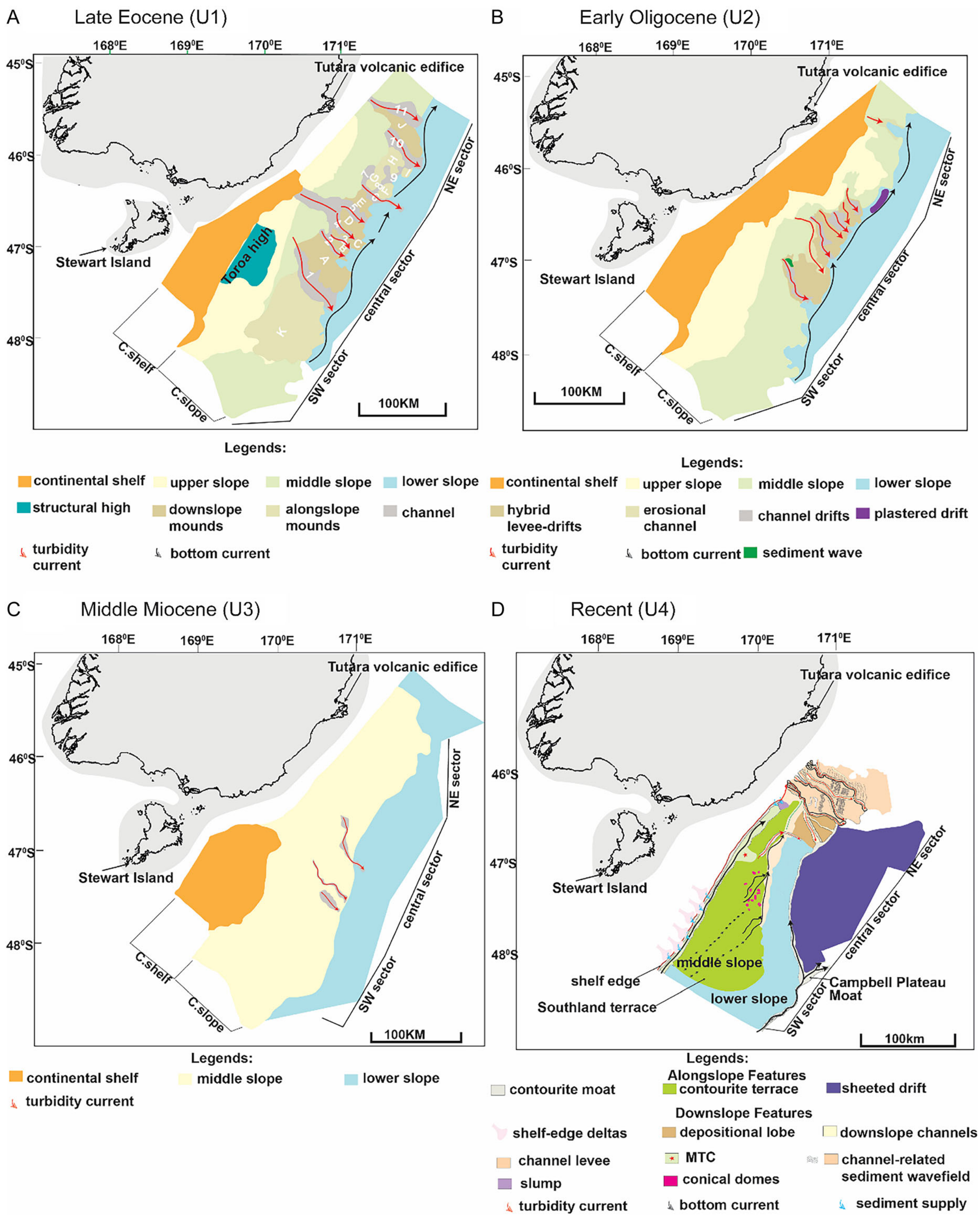

FIGURE 12 | Morpho-sedimentary maps illustrating the various erosional and depositional features that were formed along the GSB since the Middle Eocene.

5 | Discussion

5.1 | Characteristics of the Paleogene Mixed System

Our observations above indicate that the New Zealand continental slope of the South Island in the GSB has been influenced by both alongslope bottom currents and downslope turbidity currents since Middle Eocene times. We identify many characteristics of the depositional system and its morphological elements that are considered diagnostic of mixed systems elsewhere in the world (Fonnesu et al. 2020; Miramontes et al. 2021; Rodrigues, Hernández-Molina, et al. 2022; Rodrigues et al. 2021). There are five essential characteristics: (1) external morphology, (2) orientation, (3) lateral migration, (4) seismic facies, and (5) stacking patterns (Hernández-Molina et al. 2022a). We explore each of these in turn with reference to New Zealand's Paleogene record.

5.1.1 | External Morphology

The Paleogene system has several drifts that are distinctly contouritic in external morphology—a large elongate mounded drift (Figure 4) and a smooth plastered drift with subsidiary mounded drifts (Figure 5B). Others, with downslope and oblique-slope orientations, are smaller mounded bodies that possess an almond-shaped profile, which resembles the lateral accretion pattern of contourite drifts. This is distinct from normal turbidite levees that typically display a gull-wing-shaped or cuspate profile. Both the asymmetric and symmetric types (Figure 4B,C), with one or more crests, have most likely been modified in shape by the action of alongslope currents and are therefore considered levee-drifts.

5.1.2 | Orientation

The drifts identified in this study exhibit a range of orientations: perpendicular, oblique, and parallel to the margin (Figure 12). The variation in drift orientation across different parts of the basin reflects the dominant depositional processes at play. In areas where drifts align parallel to the margin (Figure 12), bottom currents are likely the primary shaping force. In contrast, perpendicular or oblique (Figure 12) alignments indicate significant contributions from turbidity currents, which can override or modify the influence of bottom currents. In the southwest sector, drifts are aligned parallel to the trend of the margin, indicative of a dominant bottom-current influence. In the central sector, levee-drifts are aligned either perpendicular or oblique to the margin, indicative of a downslope and/or mixed influence. In the northeast sector, the levee-drift orientation is influenced by turbidity currents, bottom currents, and an underlying fault-controlled geomorphology. As a result, the drifts in this area align parallel to the margin, similar to the southwest, but for different underlying reasons.

5.1.3 | Lateral Migration

Most mixed depositional systems display a clear pattern of unilateral migration with respect to the bottom-current flow, which may be either up-current or down-current (Rodrigues, Hernández-Molina, et al. 2022). This directed migration is a notable feature that reflects the prevailing bottom-current flow and associated sediment supply. In up-current migration, sediments transport counter to the dominant current direction, which may result from high downslope sediment supply that surpasses the sediment transport in the bottom current, or as a result of localized bottom-current reversals. Conversely, down-current migration suggests a dominance of sediment transport within the bottom current, and lesser downslope influence.

The mixed levee-drifts identified in this study reveal migration in an up-current direction (Figures 13 and S3). The bottom current flows toward the northeast at right angles to the southeast trending direction of the turbidity current channels, and the principal sedimentation occurs on the SW flank of the levee into the channel. The implication is that downslope sediment supply was abundant and diverted onto the channel margin by alongslope bottom currents. Similar scenarios have been identified along a number of continental margins (Fonnesu et al. 2020; Fuhrmann et al. 2020; Miramontes et al. 2021; Rebesco et al. 1998; Rebesco et al. 2002; Sansom 2018; Thiéblemont et al. 2020).

5.1.4 | Seismic Facies

Within-channel seismic facies are chaotic to high-amplitude short reflections at the base, overlain by layered to transparent channel-fill reflections (Figures 13 and S3). The basal reflections show a progressive lateral shift from high to low amplitude from the central axis to off-axis, indicative of lateral shift of facies from coarser-grained axial to finer-grained off-axial. Similar character of gradual amplitude dimming is well documented in the Mozambican (Fonnesu et al. 2020) and Nova Scotian mixed systems (Rodrigues, Deptuck, et al. 2022).

The levee-drifts seismic facies is one of low- to moderate-amplitude, well-layered reflections that pass laterally into sigmoid clinoform reflections (Figures 13 and S3). They are subparallel across the levee-drift and show a sigmoid progradational encroachment from the levee-drift crest into the channel axis—from NE toward the SW.

5.1.5 | Stacking Pattern

The seismic facies noted above show a very consistent stacking pattern. The levee-drift seismic reflections consistently migrate southwestward into and over the adjacent channel along the entire observable length. The basal channel facies also migrates to the southwest. Both are aggradational in their stacking pattern resulting in lateral accretion on the left-hand side of the channel and aggradational migration of the channel toward its right-hand side (Figures 13 and S3).

Most turbidity current channel systems show a more variable stacking pattern due to frequent alterations of the channel axis resulting from recurring lateral shifts (Fonnesu et al. 2020). These shifts are commonly linked to sinuous channel-levee systems and/or to within-channel deposition and obstruction. The consistent lateral stacking pattern observed in the New Zealand channels and channel levee-drifts (Figure 13) is interpreted as evidence for the influence of sediment deflection due to strong bottom current action in an across channel direction. In these southern hemisphere channels, the sense of deflection is enhanced by the Coriolis Effect.

A similar depositional pattern was documented in the northern South China Sea margin. Gong, Wang, Steel, et al. 2016 attributed the deposition of accreting clinoforms along one side of the channel to be controlled by bottom-current-induced helicoidal flow circulation, which induces the deep-water channel to migrate and stack in one direction. In this case, erosion occurs on the left side while deposition develops on the right side, typical of the northern hemisphere. This case also emphasizes the significance of the Coriolis Effect as well as bottom-current deflection.

The collected evidence (Figure 13) noted above serves as diagnostic indicators for simultaneous interactions between turbidity currents and bottom currents. A northeast-flowing bottom current linked with intermediate water masses is inferred here to be responsible for the observed interactions. This current has flowed alongslope at least since the Middle Eocene. The flow interaction resulted in significant flow-stripping, where the higher, more turbulent section of the turbidity current (i.e., the portion laden with suspended fine-grained sediments) is diverted by the alongslope bottom current. As a consequence, this fine-grained suspension cloud is transported northeastward away

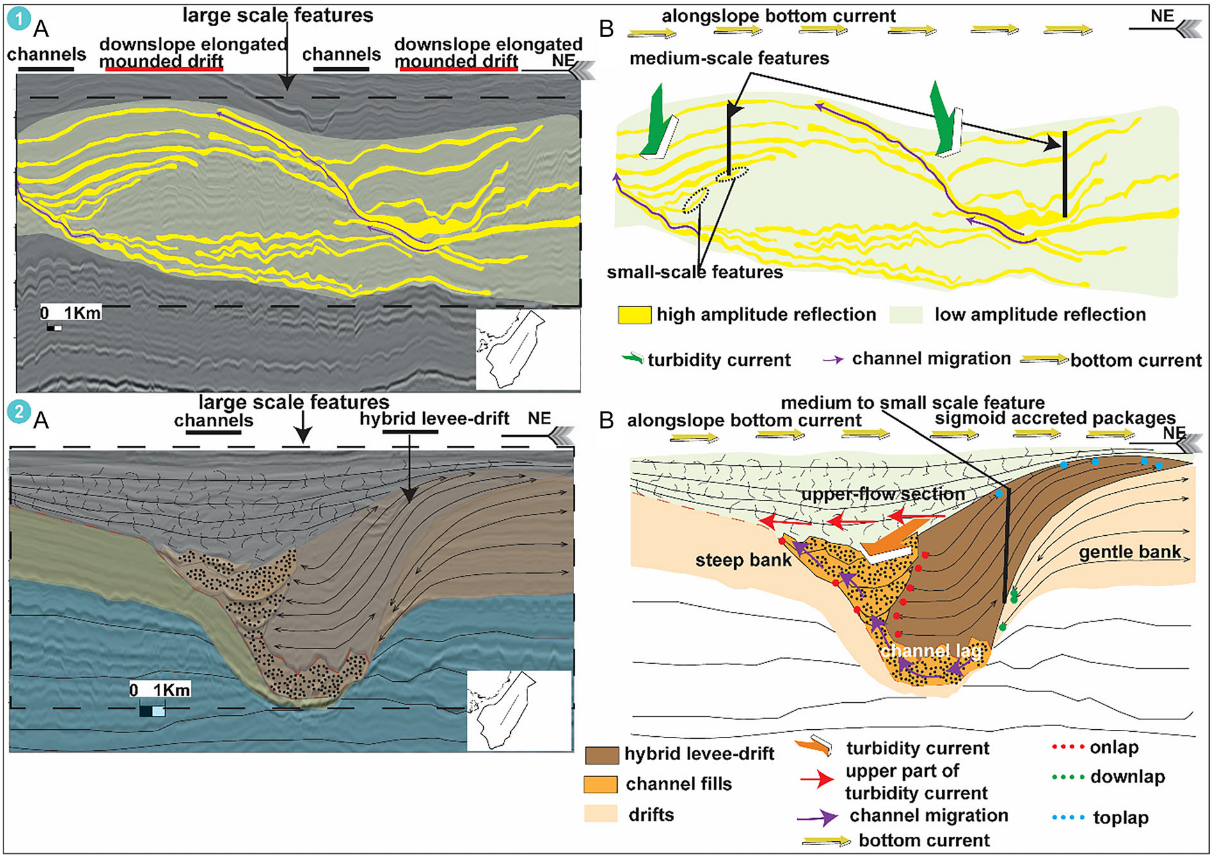

FIGURE 13 | Seismic stratigraphic interpretation of the Eocene–Oligocene record of the SE New Zealand margin at three different scales: large, medium, and small scale.

from the downslope turbidity current, and plastered against the aggrading levee-drift. As a result, this mechanism produces asymmetrical levee-drift mounds (Figures 13 and S3), rather than the typical bilateral levees that grow symmetrically on both sides of a channel due to lateral overspill from turbidity currents.

Moreover, the interplay between down-slope turbidity currents and alongslope bottom currents has greatly affected sediment deposition patterns and channel migration in our study area. This dynamic interaction explains the consistent and one-directional offset stacking observed in both large- and medium-scale sedimentary sequences. In this situation, the channel system shows a lateral migration toward the south, moving opposite to the prevailing bottom current. This southward shift is aided by the sideways buildup of fine-grained sediments within drift mounds, located on one side of the channel. As these fine sediments accumulate, they effectively confine the paths of subsequent turbidity flows, acting as natural barriers. The presence of these aggrading sediment deposits forces the channel axis to shift sideways. This lateral deflection causes the channel system to systematically migrate southwestward.

The GSB mixed system compares closely with other well-documented global examples, where channels and mounded drifts interact to shape margin architecture. Like the Cretaceous record of Argentina (Rodrigues et al. 2021) and the Upper Cretaceous to Paleogene system of Tanzania (Fuhrmann et al. 2020; Sansom 2018), the GSB exhibits large asymmetric drifts flanking erosional channels (channels that are erosional and depositional in configuration). Its oblique drift orientations (Figure 12) and southwest-directed channel migration (Figure 13) parallel features of the Eocene to Oligocene system of Mozambique (Chen et al. 2020; Fonnesu et al. 2020) and the Miocene to Recent succession of SE Greenland (Rasmussen et al. 2003), while its scale and stacking patterns are comparable to modern mixed systems in Borneo (Nugraha and Maulin 2025). Together, these similarities highlight that the GSB fits within the spectrum of globally recognized mixed turbidite to contourite systems, while its consistent oblique stacking and alongslope to downslope coupling mark it as regionally distinctive.

The lateral migration and stacking patterns observed in the GSB are consistent with trends described in other mixed systems globally. Channel-levee complexes (Figure 13) in the GSB show consistent migration to the southwest with some localized aggradation. This pattern is similar to laterally migrating channels with hybrid levees in the Pearl River Mouth Basin, South China Sea (Gong et al. 2013), the Congo channels (Gong, Wang, Steel, et al. 2016), and canyons in SE Australia (Harishidayat et al. 2024). Similarly, their oblique drift migration configuration is similar to patterns in the Mozambique Channel (Fonnesu et al. 2020; Miramontes et al. 2021) while differing from systems with little or variable migration such as Nova Scotia (Deptuck and Kendell 2020; Rodrigues, Deptuck, et al. 2022) and NE Brazil (Alves et al. 2023). A similar oblique margin drift migration pattern can also be drawn from the adjacent Canterbury Basin (Lu et al. 2003), further reinforcing that the GSB exhibits both globally typical features and regionally distinctive stacking patterns.

5.2 | Characteristics of the Neogene–Recent Mixed System

The continental slope of the GSB continued to be influenced by both alongslope and downslope processes throughout the Neogene and Quaternary periods. However, the effects of these processes appear to be more distinctly separated than during development of the Paleogene mixed system—alongslope processes dominate in the southwest and central sectors, and downslope processes in the northeast sector. The principal morphological elements and their origin are discussed below.

5.2.1 | Southland Contourite Terrace

The development of contourite terraces has been attributed to various mechanisms, including geostrophic bottom currents, eddies, and internal waves generated at water mass interfaces (Preu et al. 2013; Wilckens et al. 2021; Yin et al. 2019). The contourite terrace in the GSB, herein called the Southland Terrace, is a prominent mixed erosional and depositional feature, situated on the middle slope at water depths of 600–800 m (Figure 14). Hydrographic analysis (Figures 5 and 14) reveals that the terrace lies along the pathway of the SC and near the interface between Subantarctic Water and Antarctic Intermediate Water. Such water mass interfaces are characterized by steep vertical density gradients due to marked temperature and salinity contrasts. These zones are associated with a high degree of turbulence, which plays a significant role in erosion and sedimentation patterns on the terrace. These processes are further strengthened by the SC, which extends down to the terrace floor. Driven by wind stresses and steep vertical sea surface temperature gradients, this current generates high velocities, creating a dynamic and energetic environment in the uppermost 500–600 m of the water column. Evidence of the dynamic environment is reflected in the sedimentary characteristics on the proximal part of the Southland Terrace, where toplap terminations on seismic reflections point to erosional processes while downlap termination on the distal section suggest deposition (Figure 3C). Supporting this interpretation, seismic oceanographic sections across the terrace reveal distinct lens-shaped, bowl-like reflective features. Gorman et al. (2018) identified these features as sub-mesoscale eddies formed by the upwelling of cold, dense Subantarctic Mode Water, creating abrupt density contrasts with the overlying water mass and enhancing turbulence in the region. The Subantarctic Mode Water is a circumpolar feature of the Subantarctic Zone, forming through deep winter mixing over the Campbell Plateau (Chiswell et al. 2021 and references therein).

5.2.2 | Southland Contourite Moat

Moats are erosional features commonly associated with mounded drifts, typically forming in areas with high slope relief or near topographic barriers that guide and intensify bottom currents (Hernández-Molina et al. 2008; Miramontes et al. 2021). These features often occur at water mass interfaces, where deflected currents become stronger and more turbulent, triggering secondary processes such as helicoidal flows (Hernández-Molina et al. 2006).

In the GSB, the contourite moat, herein called the Southland Contourite Moat, is a prominent erosional feature located on the lower slope at depths of 1000–1250 m (Figure 14). It aligns

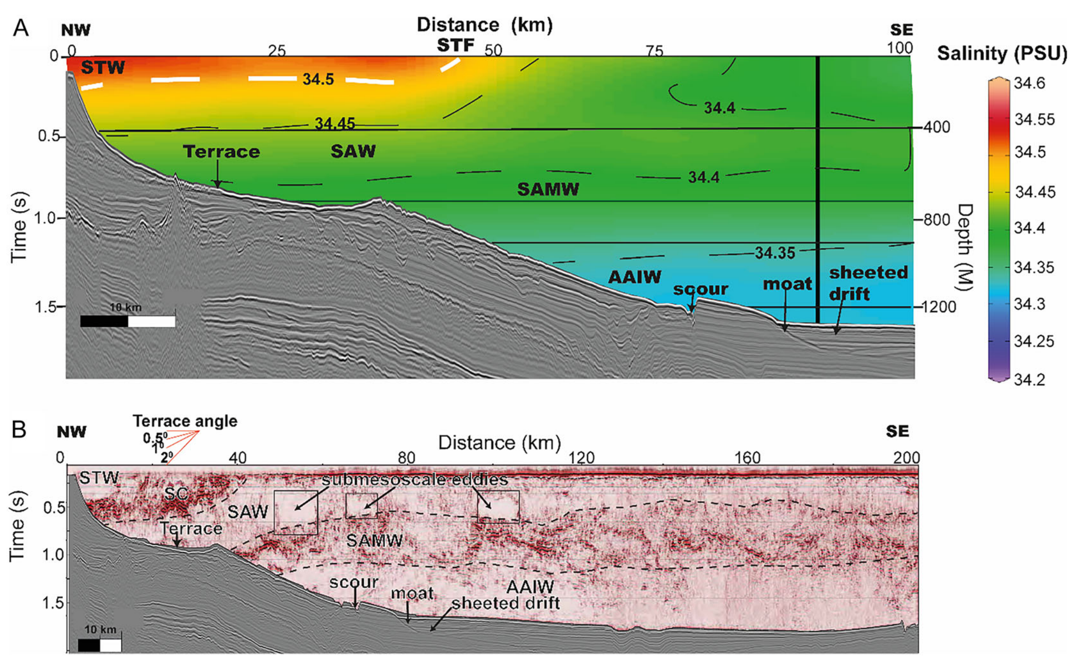

FIGURE 14 | (A) Seismic-hydrological transect, based on salinity-depth measurements taken across the slope of the GSB, and the corresponding morphosedimentary sectors developed on this margin. Salinity data from Ocean Data View (ODV) (Schlitzer 2020). Location of seismic lines shown in Figure 1. (B) Processed migrated section of OMV8-42 (Gorman et al. 2018) overlain with seismic time section of the same survey to reveal oceanographic features. The sections have been divided into water mass regions based on reflectivity and interpretation of area where the various morphological features occur. The continuous high-amplitude reflection seen at the surface in line OMV-08-42 has been identified as a surface layer (SL). STW, subtropical water; SAW, sub-Antarctic water; SAMW, sub-Antarctic mode water; AAIW, Antarctic Intermediate Water; transparent reflections bounded in black box are possible eddies.

with the path of Antarctic Intermediate Water (AAIW) and is likely influenced by a strong intermediate-depth current. Seismic data reveal its erosional nature, with well-stratified, parallel reflections truncating against the moat walls (Figures 6 and 14). In this case, the moat is found adjacent to a very low-mounded or sheeted drift, rather than a more prominent mounded drift.

5.2.3 | Slope Canyons

A series of slope canyons have developed through the Neogene to Recent in the GSB. Two primary mechanisms govern canyon development: retrogressive slope failures, which form shelf-indenting canyons, and turbidity currents, which deepen and extend canyon systems. These processes are influenced by the interaction of tectonic, sedimentary, and oceanographic factors. Where bottom currents are active, they can serve to further sculpt and modify canyon systems.

Tectonic activity plays a key role in determining canyon location and orientation by creating structural pathways for incision. On the New Zealand margin, canyon profiles exhibit steep gradients exceeding 11° and convex-upward topography, features indicative of tectonic influences. Such gradients enhance slope instability, triggering mass movements, and retrogressive downcutting that result in amphitheater-shaped canyon heads. Similar processes have been observed in the Cook Strait Canyon on the Hikurangi Margin (Micallef et al. 2012; Mountjoy et al. 2009).

Evidence of turbidity currents shaping canyon morphology is highlighted by the presence of terraces, which reflect dynamic erosional processes contributing to canyon incision and wall instability. Terraces, characteristic of submarine canyon systems, preserve a record of canyon incision and meander evolution (Deptuck et al. 2003).

In this study, terraces are commonly observed on the eastern outer bends of canyons, with well-stratified seismic reflections overlying chaotic facies at their base (Figure 11A). This configuration suggests their formation began with slope failures, such as slides or slumps, and was subsequently modified by progressive canyon incision and lateral migration. Similar features have been identified in other canyon systems, illustrating the interplay between sediment failure, turbidity currents, and depositional processes in shaping canyon morphology over time (Babonneau et al. 2010; Clark and Pickering 1996; Friedmann 2000; Hansen et al. 2017).

5.3 | Development of a Mixed Depositional System

Four main stages of evolution can be outlined for the Mid-Eocene to Recent succession of the GSB (Figures 12 and 15): (1) onset and development of a mixed system, (2) vertical growth stage, (3) inactive/burial stage, and (4) development of a new contourite system.

5.3.1 | Onset and Development (45–33.7 Ma)

From the Mid-Eocene to the Late Eocene (~45–33.7 Ma), seismic unit 1 (U1) documents the initiation of a mixed turbidite–contourite system along the middle continental slope. U1 is marked by downslope submarine channels and elongated levee-drifts in the middle sector (Figures 4 and 5). The channels show preferential migration to the SW while the levee-drifts show aggradation and slight progradation to the NE. The extension of HARs from the channels (Figure 13) and the progressive fading of the reflection draping onto the NE mounded levee-drift suggest a syndepositional interaction between NE-directed bottom-current and SE-directed turbidity flows. The bottom-current influence appears relatively weak at this stage and the levee-drifts under strong turbidity current control.

Further SW, the presence of a relatively large and thick mounded contourite drift, with a subsidiary drift at its distal end, supports the interpretation of bottom-current activity, perhaps splitting into an east directed and northeast directed flow that contour around the drift. The sediment supply to this contourite drift is most likely from the adjacent Campbell Plateau by alongslope transport, especially as there was no obvious terrestrial supply at that time. The basin is known to have experienced gradual thermal subsidence at this time, which created long-lasting accommodation space and was therefore able to trap large amounts of sediment (Cook et al. 1999).

Hemipelagic settling associated with weaker bottom-current activity led to aggradation and the development of a plastered contourite drift. A rise in sea level through the Eocene further promoted hemipelagic deposition. The higher sea levels resulted in marine transgression and landward retreat of the shoreline (Cook et al. 1999). Elongated mounded drifts were in existence in the central and SW sector, prior to the deposition of U1 (Figures 3B and 4E). Although not the focus of this study, their eastward-oriented crests strongly support the existence of a northeast-flowing bottom current.

The current that formed this mixed system was most likely associated with intermediate water masses, mainly comprising an early AAIW and Sub-Antarctic Mode Water (SAMW). In order to check this hypothesis, the depth of the seafloor (~1000 ms) was subtracted from the depth of the R6 reflection (~2100 ms) in order to obtain the average water depth (around ~1000 ms in time or ~750 m in depth) at the time of deposition of this mixed system. This estimate represents a minimum value, as tectonic subsidence and sediment compaction since R6 are expected to have increased paleowater depths by several tens to a few hundred meters, consistent with backstripping and decompaction results from the nearby South Island and Canterbury Basin (e.g., IODP Exp. 317; Christie 2007; Dvorak et al. 2024; Fulthorpe et al. 2010). This depth supports the hypothesis that the bottom current was associated with intermediate waters, as SAMW and AAIW tend to flow within these depths (700–1200 m) at present (Chiswell et al. 2021 and references therein). In addition, evidence of intermediate water circulation appears as early as ~45 Ma, particularly northbound intermediate-depth flows of AAIW circulating between the topographically constrained deep boundary current and the proto-Ross Sea gyre (Horn and Uenzelmann-Neben 2015; Huber et al. 2004; Uenzelmann-Neben et al. 2009). Prior to 45 Ma, the GSB experienced differential subsidence, which may have led southern-sourced deep western boundary bottom currents being channelled into the GSB, across the Pukaki Saddle, establishing an intermediate cyclonic flow in a clockwise direction (Sarkar et al. 2019). Evidence of this early deep western boundary current and its clockwise circulation was supported by a numerical

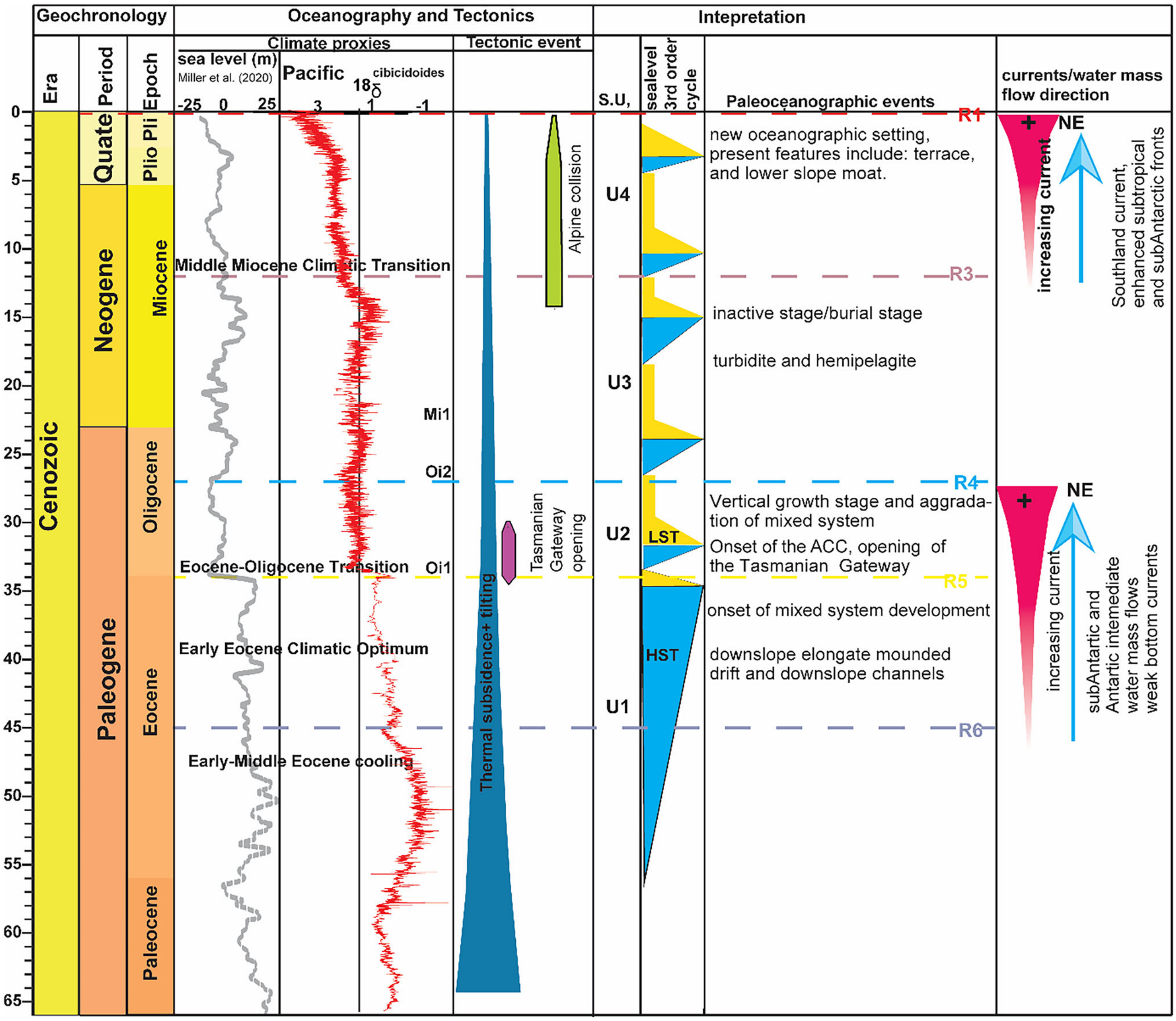

FIGURE 15 | Event chart summarizing the palaeoceanographic implications of each depositional sequence (U1U4) and facies. This shows a possible link to eustatic sea level with episodes of enhanced alongslope activity and other allogenic factors that control margin evolution. Climate proxies are represented by Cenozoic benthic foraminiferal ^{18}O and sea level records (from Miller et al. 2020); HST and LST refer to highstand systems tract (~interglacial) and lowstand systems tract (~glacial), respectively.

simulation and by the presence of cold water dinocyst diatom taxa in the sediment cores of Ocean Drilling Program (ODP) Leg 189 (Huber et al. 2004; Sijp et al. 2011). An even earlier Deep Western Boundary Current has been identified since ~65 Ma, driving drift deposition at greater depths (>2 km) (Horn and Uenzelmann-Neben 2015). This current advected southern-sourced waters further north, as a branch of that current circulated around the Campbell Plateau and entered the GSB during a period of anomalous basin subsidence (~55–45 Ma; Sutherland et al. 2010). The onset of southwest Pacific drifts occurred at ~45 Ma in the GSB, providing strong evidence for an active equatorial flow of Southern Pacific deep and intermediate waters (as the Tasmanian Gateway was still closed).

5.3.2 | Vertical Growth Stage (33.7–27 Ma)

From the Late Eocene until the Mid-Oligocene (~33.7–27 Ma), seismic unit 2 (U2) recorded continued vertical growth, which was accompanied by a transition from turbidite-dominated levee-drifts in U1 to hybrid levee-drifts with more bottom-current influence in U2. Small, confined drifts built up in the channels (Figure 4B,C), probably influenced by both bottom currents and turbidity currents. There was persistent southwest channel migration and aggradation coupled with accretionary clinoform progradation of the levee-drifts into and over the channel axes (Figure 13). This southwestward migration is consistent with deflection of turbidity currents by a northeastward flowing bottom current, in line with paleoceanographic reconstructions of proto–Antarctic circulation during the Eocene to Oligocene (Sarkar et al. 2019). We infer downslope turbidity current activity and sediment supply coupled with marked influence by alongslope bottom currents.

Most of the channels developed during U1 appear to be filled during U2 (Figure 13). The thickness attained during U2 is comparable to that of the underlying U1 and is attributable to active downslope systems supplying sediments that fill the channels as well as facilitate drift growth and aggradation. The presence of sediment waves over the levee-drifts may be the result of along-slope bottom currents and/or turbidity current overspill. The existence of plastered drifts (Figures 5B and 12B) in parts of the southeastern sector clearly suggests the operation of a continuous, active bottom-current system, which grew more robust during U2.

Taken together, the U1 to U2 transition reflects a shift driven by the Eocene to Oligocene climate transition and associated base-level change, which enhanced bottom-current circulation and slope reworking (L. Carter et al. 2004). Sediment supply was mixed, with siliciclastic input from emergent parts of southern Zealandia superimposed on background carbonate sedimentation (Cook et al. 1999), consistent with paleogeographic reconstructions that indicate recurrent onshore sources and deltaic progradation into the GSB during the Mid-Eocene to Early Oligocene (Strogen et al. 2023). Net accumulation rates remained low to moderate (250–350 m Myr^{-1}), typical of Oligocene starved margins (Christie 2007), but locally increased where channels aggraded and drifts accreted.

The lower boundary of U2 is marked by a prominent erosional surface that correlates with the Eocene–Oligocene (E/O) transition at 33.7 Ma (Figures 3 and 15), a period characterized by a major global sea-level fall of approximately 40 m drop. This regional erosional surface and gap in the stratigraphic record is known as the Marshall Paraconformity (Fulthorpe et al. 1996; Lever 2007). It has been identified in sedimentary records throughout the Tasman Sea, Lord Howe Rise, eastern South Island, and the North Chatham and Rekohu drifts, as recorded by ODP Leg 181 (Carter 1985; Fulthorpe et al. 1996; Kennett 1977; Kennett and von der Borch 1986). The onset of this erosive bottom current was driven by the opening of the Tasmanian Gateway and accompanied by associated significant climatic and oceanographic shifts (L. Carter et al. 2004; Carter and McCave 2002). The establishment of a circum-Antarctic marine circulation markedly facilitated the cooling of Antarctica and the ensuing formation of vast Antarctic ice sheets (Miller et al. 2020; Miller et al. 1991). The newly developed circum-Antarctic circulation led to further isolation of Antarctica, strengthening the cooling trend and resulting in additional climatic alterations (Carter et al. 2004). Additionally, the cooling of the Antarctic region enhanced atmospheric thermal gradients, resulting in increased wind intensity over the Southern Ocean (Carter et al. 2004). This enhanced wind activity, particularly the intensification of the westerly winds, played a crucial role in driving surface wind stress, a key factor in the initiation and strengthening of the ACC and also significant in the amplification of the proto-deep water circulation.

During glacial episodes and periods of lowered sea level, turbidity currents would have been more active on the GSB slope (Fulthorpe et al. 1996; Hutchinson et al. 2021). Coupled with enhanced bottom-current activity (Carter, McCave, et al. 2004), the margin developed as a distinct mixed turbidite–contourite system.

5.3.3 | Inactive/Burial Stage (27–12 Ma)

From the Late Oligocene until the Late Miocene (~27–12 Ma), seismic unit 3 (U3) recorded the burial of the mixed systems developed across the middle continental slope (Figure 15). The sediments deposited during U3 filled the submarine channels of the mixed system and present little to no lateral migration of either channels or levee-drifts. The channels were slowly filled with sediments and gradually transitioned toward flatter morphologies. The channel fill was accomplished by hemipelagic sedimentation in association with contribution from less active downslope and alongslope processes. Rates of sedimentation over the slope decreased as less sediment was being routed either downslope or alongslope. U3 is characterized by alternation of low- to moderate-amplitude parallel reflections, suggesting the cyclic alternation of hemipelagic processes and either weak bottom-current activity or infrequent turbidity currents. Several periods of erosion, each accompanied by accumulation of drape-like seismic facies, support this hypothesis. The drape-like facies are interpreted as hemipelagic deposits, and become more dominant upward through U3 (Figures 4–7). Accordingly, hemipelagic settling was widespread throughout the margin and dictated the morphology of the Miocene deposits.

Bottom-current circulation was inactive or less active during this period as it did not significantly affect or control sediment deposition and redistribution (Cook et al. 1999). However, localized erosion related to a regional tectonic reorganization (propagating subduction and initiation of the Alpine Fault at ~23–22 Ma) and the evolving proto–Antarctic circulation may have occurred nevertheless (Batt et al. 2004). The climate reached its optimum during this time. This optimum is most likely linked to the closure of the Indonesian Gateway between the Pacific and Indian Oceans (Bialik et al. 2019; de la Vara et al. 2013). This closure caused warm equatorial waters to be refunneled southward into the Tasman Sea (Nelson and Cooke 2001). This stage was also characterized by relative sea-level high stands (Cook et al. 1999; Fulthorpe et al. 1996), and therefore its broad and shallow shelf would have also experienced rapid evaporation. Some parts of the outer shelf and upper slope might have been exposed or the warmer climate might have led to heat exchange, which resulted in rapid evaporation of surface waters. The remaining dense sea water would have sunk, generating diffuse and less vigorous intermediate and deep waters (Brackenridge et al. 2011).

5.3.4 | A New Contourite Depositional System (12–0 Ma)

A new evolutionary stage, represented by seismic unit 4 (U4), was established in the Late Miocene to Late Pliocene, which was maintained until the present-day. U4 exhibits pronounced variability across the study area. Along the shelf off South Island, renewed sediment supply led to the development of a thick clastic wedge (Figure 3A,B). This wedge is characterized by basinward-prograding clinoforms, indicating a sustained influx of sediments and the outward growth of the shelf. The prograding clinoforms reflect the depositional processes associated with high sedimentation rates and the progressive advancement of the shelf margin into the basin over time. During this stage, sedimentation rates of 180–220 cm/kyr have been recorded in this area (Lu et al. 2005). These rates were linked to the uplift of the South Island, mountain glaciations and moderate convergence rates (Nelson et al. 2000). As global climate cooled and eustatic sea level fluctuated widely through glacial-interglacial episodes, there would have been distinct cyclicity in sediment input and across shelf transfer. The northeast sector was dominated by downslope processes.

Further south and, the southwest and central sectors of the continental slope saw the establishment of a new contourite depositional system (CDS) during the Neogene (Figures 12, 14, and 15). This comprises a contourite terrace and contourite moat across the middle slope, and a sheeted drift across the lower slope. The contourite terrace is confined by a relatively steep upper slope, and is associated with mass wasting of the adjacent continental slope. This suggests that the currents on the upper slope were strong enough to erode and undercut the continental slope, resulting in multiple submarine landslide events (Brackenridge et al. 2020; Nicholson et al. 2020). This may represent a previously unrecognized submarine hazard in this area.

These features are indicative of dynamic alongslope sediment transport conditions, that existed during this period. The active currents include the northeast-flowing SC, northeast-flowing sub-Antarctic and Antarctic Intermediate Waters (AAIW) and their associated cyclonic gyres (Figure 1).

5.4 | Mixed System Depositional Models

Two depositional models are proposed for the interactions between downslope and alongslope processes that occurred during the Mid-Eocene to Early Oligocene (Figure 16).

The first model (Figure 16A) suggests that siliciclastic input into the basin was provided by active downslope gravity flows. The frequent occurrence of turbidity currents along the continental shelf margin is primarily attributed to the rapid erosion and transport of sediment from the South Island of New Zealand and from regional highs, with paleogeographic reconstructions indicating that emergent land in southern Zealandia supplied the GSB during the Mid-Eocene to Early Oligocene through recurrent onshore sources and deltaic progradation (Strogen et al. 2023). The steepness of the upper slope promoted the generation of turbidity currents and erosion of submarine channels. The accumulation of sediment at the base of slope is augmented by a sharp gradient change and associated hydraulic jump in turbidity currents (Pudsey and Camerlenghi 1998). Modification of the depositional architecture is due to bottom-current influence, with synchronous interaction between downslope gravity flows and a NE-directed bottom current. This interaction results in NE and SE redistribution of suspended fine-grained portions, stripped from the turbidity flows. This action eventually leads to the development of asymmetric mounded levee-drifts between the submarine channels, as observed on this margin (e.g., Figures 4 and 11).

Turbidites deposited within the channels and in proximity to channel mouths also undergo winnowing and reworking as a result of bottom-current activity. This asynchronous interaction eventually leads to redistribution and redeposition of sediment along the course of the bottom currents.

Moreover, bottom-current reworking and redistribution along the margin exerts a strong influence on lateral migration of the channels and on the evolution of the asymmetric levee-drifts. This effect is principally a result of synchronous interaction, and is recorded along the channel axes, where HARs gradually reduce in thickness and amplitude as they extend laterally into the adjacent drifts. This model is similar to that proposed for the Antarctic Peninsula Pacific margin and the South China Sea (Creaser et al. 2017; Hernández-Molina et al. 2017; Rebesco et al. 2002; Wang et al. 2023).

The second model (Figure 16B) relates to the NE part of the margin and, more specifically, the Mid-Eocene to Early Oligocene turbidite–contourite system developed in this sector. The model suggests a strong bottom current interacting synchronously with frequent turbidity currents. Considering the size, internal seismic configuration, and elongation of the giant drifts within this sector, it is possible to infer that they are mostly composed of muddy sediments. On this part of the margin, it is furthermore evident that eastward-directed submarine channels were captured by a margin-parallel moat formed in between two separated drifts and deflected northward (Figure 16B). The channels terminate against two distinct moats, suggesting a strong control of bottom currents, overwhelming the turbidity currents. Normal faults below the channel could have diverted the bottom current around channel ridges and thus led to the strengthening of the bottom current. Therefore, the Mid-Eocene to Oligocene mixed system established in the NE sector of the margin shows a mixed turbidite–contourite system strongly controlled by the topography of the drift. The model reflects coeval interaction between bottom currents and turbidity currents. However, the morphological features developed across the NE sector (such as the giant mounded drifts and margin-parallel moats) suggest that this system corresponds to a contourite-dominated mixed

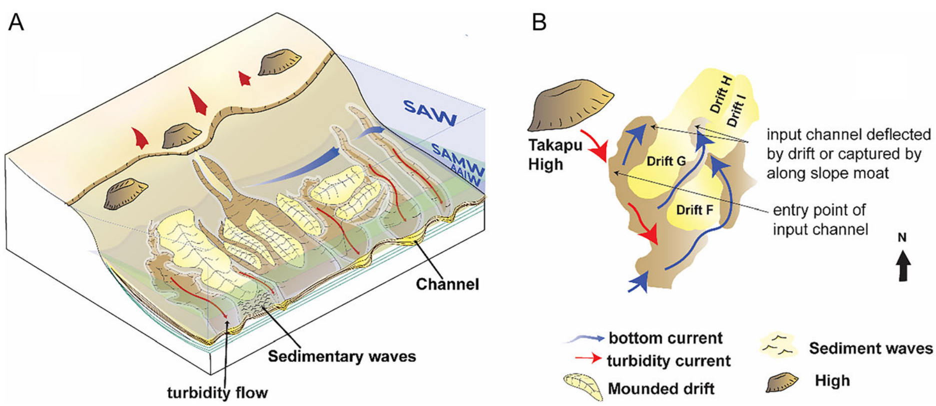

FIGURE 16 | Model of the Late Eocene mixed depositional system developed along the (A) central sector, (B) northeast sector of the New Zealand continental slope, formed by interactions between downslope gravity flows and alongslope bottom currents.

system, with the development of slope-plastered drifts developed from the pirating of fine-grained material carried in suspension by turbidity currents and by reshaping any turbidites that have collected along the contourite moats. This model aligns closely with the configuration proposed for the Tanzanian margin and Mozambique Channel (Fonnesu et al. 2020; Sansom 2018), where channels remain deflected by contour currents.

6 | Conclusions

This work described the Eocene–Present evolution of the southeast New Zealand margin, focused on the process interaction that led to the development of a mixed depositional system along the GSB. The mixed system resulted from both synchronous and asynchronous interactions between alongslope (bottom current) and downslope (turbidity current) processes. In the central area of the basin, downslope turbidity currents exerted the strongest influence on the depositional system, while alongslope processes were more influential toward the northeast. In the southwest, the system was entirely dominated by alongslope processes with no or very little influence from turbidity currents. Despite differences in dominant processes, these mixed systems all exhibited down-current migration, with only a few exceptions showing up-current migration. The final distribution of morphological elements and the lateral migration of the system reflect not only the imprint of the most influential process but also the balance of velocity, frequency, and timing between the two processes and, more significantly, the influence of variations in sediment supply.

The margin has undergone four different evolutionary stages from Mid-Eocene to Recent. The onset stage, Mid- to Late Eocene, was characterized by predominantly by gravity-driven downslope processes and the onset of levee-drift growth. This was followed by a more active vertical growth stage, with levee-drift aggradation in the Early to Late Oligocene, marked by an increased influence of bottom currents and enhanced downslope sediment supply. The subsequent burial stage, Late Oligocene to Mid-Miocene, involved the burial of earlier depositional features, possibly resulting from changes in sediment supply and/or sea level fluctuation. Finally, from Mid-Miocene to Recent, the development of a more prominent CDS signified the establishment of a new oceanographic scenario dominated by strong bottom currents.

This study of mixed systems developed along the southeast New Zealand continental margin represents the first holistic overview of the margin and advances our understanding of the interaction between alongslope and downslope processes. The two depositional models developed herein show process interaction on this particular margin. Although elements of the models may be applicable elsewhere, every margin will show its own unique character.

Funding

Niger Delta Development Commission as the funding source for the PhD of first author, Onyekachi Noble Ibezim. No other funding sources to acknowledge. There is no specific funding grant ID.

Data Availability Statement

Supplemental data is lodged with zenodo.org: https://zenodo.org/uploads/17225110?token=eyJhbGciOiJIUzUxMiJ9.eyJpZCI6ImIyOWM3ZjUwLWU1ZDYtNDFiOC05Njc2LTRjYTA3MjA4ZTZiMyIsImRhdGEiOnt9LCJyYW5kb20iOiIwZDg2YjczNDQ2NDQxMjIzNjQ2MTRlNmQyNDJmNDQzNCJ9.eRDXUMPo1jRVDLZoKeU-XZSb4sBjM6790cPT-JS-1CuPFY3eUaQnyOItNdUYIDvZi8ei8oKlrBcbJg7ZlMiysQ. *Seismic data* is open access from the New Zealand Geological Survey database at: https://www.nzpam.govt.nz/maps-geoscience/minerals-datapack. *All other data* is freely available in the PhD thesis by O. N. Ibezim (2025) entitled *Mixed depositional systems and margin evolution, South Island, New Zealand.* This is in electronic format with Heriot Watt University, Edinburgh, UK.

References

Alves, D. P., V. Maselli, D. Iacopini, A. R. Viana, and L. Jovane. 2023. "Oceanographic Exchanges Between the Southern and Northern Atlantic during the Cenozoic Inferred from Mixed Contourite-Turbidite Systems in the Brazilian Equatorial Margin." *Marine Geology* 456: 106975. https://doi.org/10.1016/j.margeo.2022.106975.

Babonneau, N., B. Savoye, M. Cremer, and M. Bez. 2010. "Sedimentary Architecture in Meanders of a Submarine Channel: Detailed Study of the Present Congo Turbidite Channel (Zaiango Project)." *Journal of Sedimentary Research* 80, no. 10: 852–866. https://doi.org/10.2110/jsr.2010.078.

Bache, F., N. Mortimer, R. Sutherland, et. al. 2014. "Seismic Stratigraphic Record of Transition from Mesozoic Subduction to Continental Breakup in the Zealandia Sector of Eastern Gondwana." *Gondwana Research* 26: 1060–1078.

Barker, P. F., G. M. Filippelli, F. Florindo, E. E. Martin, and H. D. Scher. 2007. "Onset and Role of the Antarctic Circumpolar Current." *Deep Sea Research Part II: Topical Studies in Oceanography* 54: 2388–2398. https://doi.org/10.1016/j.dsr2.2007.07.028.

Batt, G. E., S. L. Baldwin, M. A. Cottam, P. G. Fitzgerald, M. T. Brandon, and T. L. Spell. 2004. "Cenozoic Plate Boundary Evolution in the South Island of New Zealand: New Thermochronological Constraints." *Tectonics* 23: TC4001. https://doi.org/10.1029/2003TC001527.

Bialik, O. M., M. Frank, C. Betzler, R. Zammit, and N. D. Waldmann. 2019. "Two-Step Closure of the Miocene Indian Ocean Gateway to the Mediterranean." *Scientific Reports* 9: 8842.

Bostock, H., C. Jenkins, K. Mackay, et al. 2019. "Distribution of Surficial Sediments in the Ocean around New Zealand/Aotearoa. Part B: Continental Shelf." *New Zealand Journal of Geology and Geophysics* 62: 24–45. https://doi.org/10.1080/00288306.2018.1523199.

Brackenridge, R. E., U. Nicholson, B. Sapiie, D. Stow, and D. R. Tappin, 2020. *Indonesian Throughflow as a Preconditioning Mechanism for Submarine Landslides in the Makassar Strait*, Vol. 500. 195–217. Geological Society, London, Special Publications. https://doi.org/10.1144/SP500-2019-171.

Brackenridge, R., D. A. V. Stow, and F. J. Hernández-Molina. 2011. "Contourites Within a Deep-Water Sequence Stratigraphic Framework." *Geo-Marine Letters* 31: 343–360. https://doi.org/10.1007/s00367-011-0256-9.

Campbell, C. D., and D. C. Mosher. 2016. "Geophysical Evidence for Widespread Cenozoic Bottom Current Activity from the Continental Margin of Nova Scotia, Canada." *Marine Geology* 378: 237–260. https://doi.org/10.1016/j.margeo.2015.10.005.

Carter, L., and I. N. McCave. 2002. "Eastern New Zealand Drifts, Miocene-Recent." *Geological Society, London, Memoirs* 22: 385–407. https://doi.org/10.1144/gsl.Mem.2002.022.01.27.

Carter, L., R. M. Carter, and I. N. McCave. 2004. "Evolution of the Sedimentary System Beneath the Deep Pacific Inflow off Eastern

New Zealand." *Marine Geology* 205, no. 1–4: 9–27. https://doi.org/10.1016/S0025-3227(04)00016-7.

Carter, R. 1985. "The Mid-Oligocene Marshall Paraconformity, New Zealand: Coincidence with Global Eustatic Sea-Level Fall or Rise?" *Journal of Geology* 93: 359–371.

Carter, R. M. 1988. "Plate Boundary Tectonics, Global Sea-Level Changes and the Development of the Eastern South Island Continental Margin, New Zealand, Southwest Pacific: The Existence of the Widely Acclaimed Vail (Sea-Level) Curves Seems to Be Encouraging a Circularity in Arguments about Local Correlation… and Is Certainly Discouraging Attempts to Investigate Local Departures from the So-Called Global Standard. (Miall, 1986, p. 131)." *Marine and Petroleum Geology* 5: 90–107.

Carter, R. M., and L. Carter. 1996. "The Abyssal Bounty Fan and Lower Bounty Channel: Evolution of a Rifted-Margin Sedimentary System." *Marine Geology* 130: 181–202. https://doi.org/10.1016/0025-3227(95)00139-5.

Carter, R. M., C. S. Fulthorpe, and H. Lu. 2004. "Canterbury Drifts at Ocean Drilling Program Site 1119, New Zealand: Climatic Modulation of Southwest Pacific Intermediate Water Flows since 3.9 Ma." *Geology* 32, no. 11: 1005–1088.

Carter, R. M., I. N. McCave, and L. Carter. 2004. "Leg 181 Synthesis: Fronts, Flows, Drifts, Volcanoes, and the Evolution of the Southwestern Gateway to the Pacific Ocean, Eastern New Zealand." In *Proceedings of the Ocean Drilling Program, Scientific Results*, edited by C. Richter, Vol. 181, pp. 1–111. Ocean Drilling Program. https://doi.org/10.2973/odp.proc.sr.181.210.2004.

Carter, R. M., L. Carter, J. Williams, and C. A. Landis. 1985. *Modern and Relict Sedimentation on the Otago Continental Shelf*. New Zealand Oceanographic Institute Memoir, No. 93, Null. New Zealand Oceanographic Institute. 43 pp.

Chen, Y., G. Yao, X. Wang, et al. 2020. "Flow Processes of the Interaction Between Turbidity Flows and Bottom Currents in Sinuous Unidirectionally Migrating Channels: An Example from the Oligocene Channels in the Rovuma Basin, Offshore Mozambique." *Sedimentary Geology* 404: 105680. https://doi.org/10.1016/j.sedgeo.2020.105680.

Chiswell, S. M., H. C. Bostock, P. J. H. Sutton, and M. J. M. Williams. 2021. "Physical Oceanography of the Deep Seas around New Zealand: A Review." *New Zealand Journal of Marine and Freshwater Research* 49: 286–317. https://doi.org/10.1080/00288330.2014.992918.

Christie, L. J. 2007. "Cretaceous and Cenozoic Basin Evolution Based on Decompacted Sediment Thickness from Petroleum Wells around New Zealand." Doctoral diss., Open Access Te Herenga Waka-Victoria University of Wellington, School of Geography, Environment and Earth Science.

Clark, J. D., and K. T. Pickering. 1996. *Submarine Channels: Processes and Architecture*. Vallis Press.

Constable, R., and R. Crookbain. 2011. *A Sequence Stratigraphic Study of the Great South Basin. 4348*. Ministry of commerce.

Constable, R., S. Langdale, and T. Allan. 2013. "Development of a Sequence Stratigraphic Framework in the Great South Basin." *Science* 3: 1–21.

Cook, R. A., R. Sutherland, and H. Zhu. 1999. *Cretaceous-Cenozoic Geology and Petroleum Systems of the Great South Basin, New Zealand*, Vol. 20. Institute of Geological & Nuclear Sciences Monograph, Institute of Geological & Nuclear Sciences.

Cox, S. C., and R. Sutherland. 2007. "Regional Geological Framework of South Island, New Zealand, and its Significance for Understanding the Active Plate Boundary." In *Geophysical Monograph Series*. Vol. 175, 19–46. American Geophysical Union.

Creaser, A., F. J. Hernández-Molina, G. Badalini, et al. 2017. "A Late Cretaceous Mixed (turbidite-Contourite) System along the Uruguayan Margin: Sedimentary and Palaeoceanographic Implications." *Marine Geology* 390: 234–253. https://doi.org/10.1016/j.margeo.2017.07.004.

de la Vara, A., P. T. Meijer, and M. Wortel. 2013. "Model Study of the Circulation of the Miocene Mediterranean Sea and Paratethys: Closure of the Indian Gateway." *Climate of the Past Discussions* 9: 4385–4424.

Deng, X., K. Huang, and X. Li. 2024. "Sedimentary Characteristics and Evolution of the Late Miocene to Quaternary Tributary Channels in the Head of Bounty Channel, New Zealand." *Applied Sciences* 14: 6160. https://doi.org/10.3390/app14146160.

Deptuck, M. E., G. S. Steffens, M. Barton, and C. Pirmez. 2003. "Architecture and Evolution of Upper Fan Channel-Belts on the Niger Delta Slope and in the Arabian Sea." *Marine and Petroleum Geology* 20: 649–676.

Deptuck, M., and K. Kendell. 2020. *Atlas of 3D Seismic Surfaces and Thickness Maps, Central and Southwestern Scotian Slope*. Geoscience Open File Report.

Dvorak, K., M. Kominz, and M. Crundwell. 2024. "Tectonic Subsidence and Uplift Within Canterbury Basin, South Island, New Zealand." *New Zealand Journal of Geology and Geophysics* 67: 409–425.

Eagles, G., K. Gohl, and R. D. Larter. 2004. "High-Resolution Animated Tectonic Reconstruction of the South Pacific and West Antarctic Margin." *Geochemistry, Geophysics, Geosystems* 5, no. 7: 1–21, Q07002. https://doi.org/10.1029/2003GC000657.

Embry, A. F. 2009. "Practical Sequence Stratigraphy." *Canadian Society of Petroleum Geologists* 81: 79.

Fierens, R., L. Droz, S. Toucanne, et al. 2019. "Late Quaternary Geomorphology and Sedimentary Processes in the Zambezi Turbidite System (Mozambique Channel)." *Geomorphology* 334: 1–28.

Fonnesu, M., D. Palermo, M. Galbiati, M. Marchesini, E. Bonamini, and D. Bendias. 2020. "A New World-Class Deep-Water Play-Type, Deposited by the Syndepositional Interaction of Turbidity Flows and Bottom Currents: The Giant Eocene Coral Field in Northern Mozambique." *Marine and Petroleum Geology* 111: 179–201. https://doi.org/10.1016/j.marpetgeo.2019.07.047.

Friedmann, S. 2000. "*Recent advances in deep-water sedimentology and stratigraphy using conventional and high-resolution 3D seismic data*." In Conference CD with Extended Abstracts. GeoCanada.

Fuhrmann, A., I. A. Kane, E. Schomacker, M. A. Clare, and A. Ponten. 2022. "Bottom Current Modification of Turbidite Lobe Complexes." *Frontiers in Earth Science* 9: 752066. https://doi.org/10.3389/feart.2021.752066.

Fuhrmann, A., I. A. Kane, M. A. Clare, et al. 2020. "Hybrid Turbidite-Drift Channel Complexes: An Integrated Multiscale Model." *Geology* 48: 562–568. https://doi.org/10.1130/G47179.1.

Fulthorpe, C. S., K. Hoyanagi, P. Blum, et al. 2010. "*Integrated Ocean Drilling Program Expedition 317 preliminary Report Canterbury Basin Sea Level Global and Local Controls on Continental Margin Stratigraphy*." Integrated Ocean Drilling Program: Preliminary Reports. 1–133.

Fulthorpe, C. S., R. M. Carter, K. G. Miller, and J. Wilson. 1996. "Marshall Paraconformity: A Mid-Oligocene Record of Inception of the Antarctic Circumpolar Current and Coeval Glacio-Eustatic Lowstand?" *Marine and Petroleum Geology* 13: 61–77. https://doi.org/10.1016/0264-8172(95)00033-X.

Gong, C., Y. Wang, M. Rebesco, S. Salon, and R. J. Steel. 2018. "How Do Turbidity Flows Interact with Contour Currents in Unidirectionally Migrating Deep-Water Channels?" *Geology* 46: 551–554. https://doi.org/10.1130/g40204.1.

Gong, C., Y. Wang, R. Steel, J. Peakall, X. Zhao, and Q. Sun. 2016. "Flow Processes and Sedimentation in Unidirectionally Migrating Deep-Water Channels: From a Three-Dimensional Seismic Perspective." *Sedimentology* 63, no. 3: 645–661. https://doi.org/10.1111/sed.12233

Gong, C., Y. Wang, R. Zheng, et al. 2016. "Middle Miocene Reworked Turbidites in the Baiyun Sag of the Pearl River Mouth Basin, Northern South China Sea Margin: Processes, Genesis, and Implications." *Journal of Asian Earth Sciences* 128: 116–129. https://doi.org/10.1016/j.jseaes.2016.06.025.

Gong, C., Y. Wang, W. Zhu, W. Li, and Q. Xu. 2013. "Upper Miocene to Quaternary Unidirectionally Migrating Deep-Water Channels in the Pearl River Mouth Basin, Northern South China SeaUnidirectionally Migrating Deep-Water Channels." *AAPG Bulletin* 97: 285–308.

Gorman, A. R., M. W. Smillie, J. K. Cooper, et al. 2018. "Seismic Characterization of Oceanic Water Masses, Water Mass Boundaries, and Mesoscale Eddies SE of New Zealand." *Journal of Geophysical Research: Oceans* 123: 1519–1532. https://doi.org/10.1002/2017JC013459.

Hadfield, M. G., G. J. Rickard, and M. J. Uddstrom. 2007. "A Hydrodynamic Model of Chatham Rise, New Zealand." *New Zealand Journal of Marine and Freshwater Research* 41: 239–264.

Hansen, L., M. Janocko, I. Kane, and B. Kneller. 2017. "Submarine Channel Evolution, Terrace Development, and Preservation of Intra-Channel Thin-Bedded Turbidites: Mahin and Avon Channels, Offshore Nigeria." *Marine Geology* 383: 146–147. https://doi.org/10.1016/j.margeo.2016.11.011.

Harishidayat, D., Y. Niyazi, H. Stewart, A. Al-Shuhail, and A. Jamieson. 2024. "Submarine Canyon Development Controlled by Slope Failure and Oceanographic Process Interactions." *Scientific Reports* 14, no. 1: 18486. https://doi.org/10.1038/s41598-024-69536-8.

Hernández-Molina, F. J., E. Llave, and D. A. V. Stow. 2008. "Continental Slope Contourites." In *Contourites Developments in Sedimentology*, edited by M. Rebesco and A. Camerlenghi, Vol. 60, 379–408. Elsevier. https://doi.org/10.1016/S0070-4571(08)10019-X.

Hernández-Molina, F. J., E. Llave, and D. A. V. Stow, et al. 2006. "The Contourite Depositional System of the Gulf of Cádiz: A Sedimentary Model Related to the Bottom Current Activity of the Mediterranean Outflow Water and its Interaction with the Continental Margin." *Deep Sea Research Part II: Topical Studies in Oceanography* 53: 1420–1463. https://doi.org/10.1016/j.dsr2.2006.04.016.

Hernández-Molina, F. J., R. D. Larter, and A. Maldonado. 2017. "Neogene to Quaternary Stratigraphic Evolution of the Antarctic Peninsula, Pacific Margin Offshore of Adelaide Island: Transitions from a Non-Glacial, through Glacially-Influenced to a Fully Glacial State." *Global and Planetary Change* 156: 80–111. https://doi.org/10.1016/j.gloplacha.2017.07.002.

Hernández-Molina, F. J., S. de Castro, W. de Weger, et al. 2022a. "Chapter 9 - Contourites and Mixed Depositional Systems: A Paradigm for Deepwater Sedimentary Environments." In *Deepwater Sedimentary Systems*, edited by J. R. Rotzien, C. A. Yeilding, R. A. Sears, F. J. Hernández-Molina, and O. Catuneanu, 301–360. Elsevier. https://doi.org/10.1016/B978-0-323-91918-0.00004-9.

Hernández-Molina, F. J., S. de Castro, W. de Weger, et al. 2022b. "*Contourites and Mixed Depositional Systems: A Paradigm for Deepwater Sedimentary Environments, Deepwater Sedimentary Systems*, 301–360. Elsevier.

Horn, M., and G. Uenzelmann-Neben. 2015. "The Deep Western Boundary Current at the Bounty Trough, East of New Zealand: Indications for Its Activity Already Before the Opening of the Tasmanian Gateway." *Marine Geology* 362: 60–75. https://doi.org/10.1016/j.margeo.2015.01.011.

Huber, M., H. Brinkhuis, C. E. Stickley, et al. 2004. "Eocene Circulation of the Southern Ocean: Was Antarctica Kept Warm by Subtropical Waters?" *Paleoceanography* 19, no. 4: PA4026. https://doi.org/10.1029/2004PA001014.

Hunt International Petroleum. 1977a. *Final Report Kawau-1A*. Ministry of Economic Development New Zealand.

Hunt International Petroleum. 1977b. *Pakahā-1 Well Completion Report*. Ministry of Economic Development New Zealand.

Hunt International Petroleum. 1977c. *Toroa-1 Well Completion Report. 691*. Ministry of Economic Development.

Hunt International Petroleum. 1978. *Tara-1 Well Completion Report PPL 740. PR 732*. Ministry of Economic Development.

Hutchinson, D. K., H. K. Coxall, D. J. Lunt, et al. 2021. "The Eocene–Oligocene Transition: A Review of Marine and Terrestrial Proxy Data, Models and Model–data Comparisons." *Climate of the Past* 17: 269–315.

Kennett, J. P. 1977. "Cenozoic Evolution of Antarctic Glaciation, the Circum-Antarctic Ocean, and Their Impact on Global Paleoceanography." *Journal of Geophysical Research* 82: 3843–3860.

Kennett, J. P., and C. C. von der Borch. 1986. "Southwest Pacific Cenozoic Paleoceanography." In *Initial Reports of the Deep Sea Drilling Project*, edited by J. P. Kennett and C. C. von derBorch, Vol. 90, 1493–1517. U.S. Government Printing Office. https://doi.org/10.2973/dsdp.proc.90.148.1986.

Lever, H. 2007. "Review of Unconformities in the Late Eocene to Early Miocene Successions of the South Island, New Zealand: Ages, Correlations, and Causes." *New Zealand Journal of Geology and Geophysics* 50: 245–261. https://doi.org/10.1080/00288300709509835.

Lu, H., C. Fulthorpe, and M. Kominz. 2005. "Miocene-Recent Tectonic and Climatic Controls on Sediment Supply and Sequence Stratigraphy: Canterbury Basin, New Zealand." *Basin Research* 17: 311–328. https://doi.org/10.1111/j.1365-2117.2005.00266.x.

Lu, H., C. Fulthorpe, and P. Mann. 2003. "Three-Dimensional Architecture of Shelf-Building Sediment Drifts in the Offshore Canterbury Basin, New Zealand." *Marine Geology* 193: 19–47. https://doi.org/10.1016/S0025-3227(02)00612-6.

Micallef, A., J. Mountjoy, M. Canals, and G. Lastras. 2012. *Deep-Seated Bedrock Landslides and Submarine Canyon Evolution in an Active Tectonic Margin: Cook Strait, New Zealand*, Vol. 31, 201–212. Springer. https://doi.org/10.1007/978-94-007-2162-3_18.

Miller, K. G., J. D. Wright, and R. G. Fairbanks. 1991. "Unlocking the Ice House: Oligocene-Miocene Oxygen Isotopes, Eustasy, and Margin Erosion." *Journal of Geophysical Research: Solid Earth* 96: 6829–6848.

Miller, K. G., J. V. Browning, W. J. Schmelz, R. E. Kopp, G. S. Mountain, and J. D. Wright. 2020. "Cenozoic Sea-Level and Cryospheric Evolution from Deep-Sea Geochemical and Continental Margin Records." *Science Advances* 6: eaaz1346. https://doi.org/10.1126/sciadv.aaz1346.

Miramontes, E., A. Thiéblemont, N. Babonneau, et al. 2021. "Contourite and Mixed Turbidite-Contourite Systems in the Mozambique Channel (SW Indian Ocean): Link Between Geometry, Sediment Characteristics and Modelled Bottom Currents." *Marine Geology* 437: 106502. https://doi.org/10.1016/j.margeo.2021.106502.

Mitchell, J. N., and Helen. 2012. *OS20/20 Canterbury - Great South Basin TAN1209 Voyage Report*. NIWA Client Report WLG2012-35. National Institute of Water & Atmospheric Research Ltd. (NIWA).

Mortimer, N. 2004. "New Zealand's Geological Foundations." *Gondwana Research* 7: 261–272. https://doi.org/10.1016/S1342-937X(05)70324-5.

Mortimer, N. 2020. *Zealandia (Including New Zealand and New Caledonia), Reference Module in Earth Systems and Environmental Sciences*. Elsevier. https://doi.org/10.1016/B978-0-08-102908-4.00065-5.

Mortimer, N., H. J. Campbell, A. J. Tulloch, et al. 2017. "Zealandia: Earth's Hidden Continent." *GSA Today* 27: 27–35.

Mountjoy, J. J., P. M. Barnes, and J. R. Pettinga. 2009. "Morphostructure and Evolution of Submarine Canyons across an Active Margin: Cook Strait Sector of the Hikurangi Margin, New Zealand." *Marine Geology* 260: 45–68. https://doi.org/10.1016/j.margeo.2009.01.006.

Nelson, C. S., and P. J. Cooke. 2001. "History of Oceanic Front Development in the New Zealand Sector of the Southern Ocean during the Cenozoic—A Synthesis." *New Zealand Journal of Geology and Geophysics* 44: 535–553.

Nelson, C., I. Hendy, H. Neil, C. Hendy, and P. Weaver. 2000. "Last Glacial Jetting of Cold Waters through the Subtropical Convergence Zone in the Southwest Pacific off Eastern New Zealand, and Some Geological Implications." *Palaeogeography, Palaeoclimatology, Palaeoecology* 156: 103–121.

New Zealand's Minerals and Petroleum Industry. 2016. "*Petroleum Exploration Data Pack*." https://www.nzpam.govt.nz/maps-geoscience/petroleum-datapack.

Nicholson, U., and D. Stow. 2019. "Erosion and Deposition Beneath the Subantarctic Front since the Early Oligocene." *Scientific Reports* 9: 9296. https://doi.org/10.1038/s41598-019-45815-7.

Nicholson U., S. Libby, D. R. Tappin, and D. McCarthy. 2020. "The Subantarctic Front as a Sedimentary Conveyor Belt for Tsunamigenic Submarine Landslides." *Marine Geology* 424: 106161. https://doi.org/10.1016/j.margeo.2020.106161.

Nugraha, H. D., and H. B. Maulin. 2025. "Hybrid Turbidite–contourite Systems in the Modern Tarakan Basin: Seismic Sedimentology and Analogue for Subsurface Storage." *Frontiers in Earth Science* 13: 2025. https://doi.org/10.3389/feart.2025.1614416.

Pandolpho, B. T., A. H. da Fontoura Klein, I. Dutra, et al. 2021. "Seismic Record of a Cyclic Turbidite-Contourite System in the Northern Campos Basin, SE Brazil." *Marine Geology* 434: 106422.

Pfuhl, H. A., and I. N. McCave. 2005. "Evidence for Late Oligocene Establishment of the Antarctic Circumpolar Current." *Earth and Planetary Science Letters* 235: 715–728. https://doi.org/10.1016/j.epsl.2005.04.025.

Phillips, T. B., and C. Magee. 2020. "Structural Controls on the Location, Geometry and Longevity of an Intraplate Volcanic System: The Tuatara Volcanic Field, Great South Basin, New Zealand." *Journal of the Geological Society* 177: 1039–1056. https://doi.org/10.1144/jgs2020-050.

Placid Oil. 1984. *Final Geological Well Report Pukaki-1 Great South Basin NZ PPL 38081. PR1005*. Ministry of Economic Development New Zealand.

Preu, B., F. J. Hernández-Molina, R. Violante, et al. 2013. "Morphosedimentary and Hydrographic Features of the Northern Argentine Margin: The Interplay Between Erosive, Depositional and Gravitational Processes and Its Conceptual Implications." *Deep Sea Research Part I: Oceanographic Research Papers* 75: 157–174.

Pudsey, C. J., and A. Camerlenghi. 1998. "Glacial–interglacial Deposition on a Sediment Drift on the Pacific Margin of the Antarctic Peninsula." *Antarctic Science* 10: 286–308. https://doi.org/10.1017/S0954102098000376.

Rasmussen, S., H. Lykke-Andersen, A. Kuijpers, and S. Troelstra. 2003. "Post-Miocene Sedimentation at the Continental Rise of Southeast Greenland: The Interplay Between Turbidity and Contour Currents." *Marine Geology* 196: 37–52.

Rebesco, M., A. Camerlenghi, and C. Zanolla. 1998. "Bathymetry and Morphogenesis of the Continental Margin West of the Antarctic Peninsula." *Terra Antarctica* 5: 715–725.

Rebesco, M., C. J. Pudsey, M. Canals, et al. 2002. "Sediment Drifts and Deep-Sea Channel Systems, Antarctic Peninsula Pacific Margin." *Geological Society, London, Memoirs* 22: 353–371. https://doi.org/10.1144/GSL.MEM.2002.022.01.25.

Rodrigues, S., F. J. Hernández-Molina, and A. Kirby. 2021. "A Late Cretaceous Mixed (turbidite-Contourite) System along the Argentine Margin: Paleoceanographic and Conceptual Implications." *Marine and Petroleum Geology* 123: 104768.

Rodrigues, S., F. J. Hernández-Molina, M. Fonnesu, E. Miramontes, M. Rebesco, and D. C. Campbell. 2022. "A New Classification System for Mixed (turbidite-Contourite) Depositional Systems: Examples, Conceptual Models and Diagnostic Criteria for Modern and Ancient Records." *Earth-Science Reviews* 230: 104030.

Rodrigues, S., M. Deptuck, K. Kendell, C. Campbell, and F. Hernández-Molina. 2022. "Cretaceous to Eocene Mixed Turbidite-Contourite Systems Offshore Nova Scotia (Canada): Spatial and Temporal Variability of Down-and Along-Slope Processes." *Marine and Petroleum Geology* 138: 105572.

Sahoo, T. R., D. P. Strogen, G. H. Browne, and A. Nicol. 2022. "Evolution of Syn- to Early Post-Rift Facies in Rift Basins: Insights from the Cretaceous–Paleocene of the Great South Basin, New Zealand." *Basin Research* 34: 1113–1142. https://doi.org/10.1111/bre.12652.

Sahoo, T., A. Nicol, G. Browne, and D. Strogen. 2020. "Evolution of a Normal Fault System Along Eastern Gondwana, New Zealand." *Tectonics* 39: 1–19. https://doi.org/10.1029/2020TC006181.

Sahoo, T., P. King, K. Bland, D. Strogen, R. Sykes, and F. Bache. 2014. "Tectono-Sedimentary Evolution and Source Rock Distribution of the Mid to Late Cretaceous Succession in the Great South Basin, New Zealand." *APPEA Journal* 54: 259–274. https://doi.org/10.1071/AJ13026.

Sansom, P. 2018. "Hybrid Turbidite–contourite Systems of the Tanzanian Margin." *Petroleum Geoscience* 24: 258–276. https://doi.org/10.1144/petgeo2018-044.

Sarkar, S., C. Basak, M. Frank, et al. 2019. "Late Eocene Onset of the Proto-Antarctic Circumpolar Current." *Scientific Reports* 9: 10125.

Scher, H. D., and E. E. Martin. 2006. "Timing and Climatic Consequences of the Opening of Drake Passage." *Science* 312: 428–430. https://doi.org/10.1126/science.1120044.

Schlitzer, R. 2011. *Ocean Data View*. Alfred Wegener Institute (AWI). http://odv.awi.de.

Schlitzer, R. 2020. *Ocean Data View, ODV 5.2. 1*.

Sijp, W. P., M. H. England, and M. Huber. 2011. "Effect of the Deepening of the Tasman Gateway on the Global Ocean." *Paleoceanography* 26, no. 4: PA4207. https://doi.org/10.1029/2011PA002143.

Sokolov, S., and S. R. Rintoul. 2009. "Circumpolar Structure and Distribution of the Antarctic Circumpolar Current Fronts: 1. Mean Circumpolar Paths." *Journal of Geophysical Research: Oceans* 114, no. C11: C11018. https://doi.org/10.1029/2008JC005108.

Stevens, C. L., J. M. O'Callaghan, S. M. Chiswell, and M. G. Hadfield. 2021. "Physical Oceanography of New Zealand/Aotearoa Shelf Seas – A Review." *New Zealand Journal of Marine and Freshwater Research* 55: 6–45. https://doi.org/10.1080/00288330.2019.1588746.

Strogen, D. P. K., and P. R. 2014. *A New Zealandia-Wide Seismic Horizon Naming schemeGNS Science Report 2014/34*. GNS Science Report 2014/34. GNS Science (Institute of Geological and Nuclear Sciences Limited).

Strogen, D. P., H. Seebeck, B. R. Hines, K. J. Bland, and J. S. Crampton. 2023. "Palaeogeographic Evolution of Zealandia: Mid-Cretaceous to Present." *New Zealand Journal of Geology and Geophysics* 66: 528–557. https://doi.org/10.1080/00288306.2022.2115520.

Sutherland, R., S. Spasojevic, and M. Gurnis. 2010. "Mantle Upwelling after Gondwana Subduction Death Explains Anomalous Topography and Subsidence Histories of Eastern New Zealand and West Antarctica." *Geology* 38: 155–158. https://doi.org/10.1130/G30613.1.

Sutton, P. 2001. "Detailed Structure of the Subtropical Front over Chatham Rise, East of New Zealand." *Journal of Geophysical Research: Oceans* 106: 31045–31056. https://doi.org/10.1029/2000jc000562.

Sutton, P. J. H. 2003. "The Southland Current: A Subantarctic Current." *New Zealand Journal of Marine and Freshwater Research* 37: 645–652. https://doi.org/10.1080/00288330.2003.9517195.

Thiéblemont, A., F. J. Hernández-Molina, J.-P. Ponte, et al. 2020. "Seismic Stratigraphic Framework and Depositional History for Cretaceous and Cenozoic Contourite Depositional Systems of the Mozambique Channel, SW Indian Ocean." *Marine Geology* 425: 106192. https://doi.org/10.1016/j.margeo.2020.106192.

Uenzelmann-Neben, G. 2006. "Depositional Patterns at Drift 7, Antarctic Peninsula: Along-Slope versus Down-Slope Sediment Transport as Indicators for Oceanic Currents and Climatic Conditions." *Marine Geology* 233: 49–62. https://doi.org/10.1016/j.margeo.2006.08.008.

Uenzelmann-Neben, G., J. Grobys, K. Gohl, and D. Barker. 2009. "Neogene Sediment Structures in Bounty Trough, Eastern New Zealand: Influence of Magmatic and Oceanic Current Activity." *GSA Bulletin* 121: 134–149. https://doi.org/10.1130/B26259.1.

Wang, X., B. Kneller, and Q. Sun. 2023. "Sediment Waves Control Origins of Submarine Canyons." *Geology* 51: 310–314. https://doi.org/10.1130/g50642.1.

Weaver, P. P., L. Carter, and H. L. Neil. 1998. "Response of Surface Water Masses and Circulation to Late Quaternary Climate Change East of New Zealand." *Paleoceanography* 13: 70–83.

Wilckens, H., E. Miramontes, T. Schwenk, et al. 2021. "The Erosive Power of the Malvinas Current: Influence of Bottom Currents on Morpho-Sedimentary Features along the Northern Argentine Margin (SW Atlantic Ocean)." *Marine Geology* 439: 106539. https://doi.org/10.1016/j.margeo.2021.106539.

Yin, S., F. Hernández-Molina, W. Zhang, et al. 2019. "The Influence of Oceanographic Processes on Contourite Features: A Multidisciplinary Study of the Northern South China Sea." *Marine Geology* 415: 105967. https://doi.org/10.1016/j.margeo.2019.105967.

Supporting Information

Additional supporting information can be found online in the Supporting Information section. **Supporting Fig. S1:** NW-SE hydrographic-seismic intersection across the Great South Basin. The colour gradient represents salinity variations (in PSU). The water masses comprise: STW – Subtropical Water, SAW – Sub-Antarctic Water, SAMW – Sub-Antarctic Mode Water, AAIW – Antarctic Intermediate Water, and TZ – transition zone between SAMW and AAIW. **Supporting Fig. S2:** Uninterpreted and interpreted section of a seismic profile running along the Toroa and Tara wells showing the correlation between the main discontinuities (R1, R3, R4, R5, and R6). This seismic profile is also shown in Figure 3B. The scatter diagram shows the time-depth data for these wells, and the trend line (red dashed line) used to depth-convert the data. **Supporting Fig. S3:** Seismic facies scheme devised for interpretation of depositional environments in this study. **Supporting Table S1:** Details of the main 2D seismic acquisition parameters for the Great South Basin. **Supporting Table S2:** Regional stratigraphic discontinuities defined by Constable et al. (2013), Cook (1999), Omosanya and Harishidayat (2019) and McMillan and Wilson (1997) for the Great South Basin, New Zealand continental margin. **Supporting Table S3:** Summary of the bounding discontinuities, seismic units and reflection termination patterns.